SPECIAL TOPICS

Optimizing 3D magnetic perturbations for edge instability control in the KSTAR tokamak

Jong-Kyu Park[1,2]

Abstract

A small non-axisymmetric (3D) magnetic field can offer invaluable ways for instability control in tokamaks when optimally used, as has been highlighted by the edge-localized mode (ELM) control using a resonant magnetic perturbation (RMP). While the inherent complexity due to its 3D nature constantly poses scientific challenges, recent research progresses have been increasing the prospects of universal predictive capabilities on RMP ELM suppression. A successful framework has been developed based on integrated perturbative models under international collaborations centered around the Korean Superconducting Tokamak Advanced Research (KSTAR), as will be reviewed in this article. This framework separates the interaction between 3D coils and resonant fields as the ideal magnetohydrodynamic (MHD) outer-layer process in fast time scales, from the dynamics of resonant field penetration as the narrow boundary layer process in non-ideal MHD time scales. The major profile alterations can occur only when the resonant field becomes strong enough to penetrate and bifurcate to new magnetic island topologies. This hypothesis enables simplified 3D field optimizations once the field penetration thresholds are identified. The prediction of the field penetration thresholds require non-linear MHD simulations but can be simplified by isolating it from outer-layer response, successfully explaining key parametric dependencies and accessibility conditions for RMP ELM suppression. Improved understanding has been leveraged to expand physics basis for underlying transport in fully geometry, as recent perturbative 3D simulations are revealing the complex interplays across classical and non-classical transport, between Kink and tearing mode structures, between closed- and open-field lines which are important to optimize power flux to plasma facing components. The pre-programmed predictive optimization of 3D tokamak scenarios can then be combined with an adaptive RMP control to find the optimal trade-off between stability and confinement. The above approaches under this framework are not based on the first principles but are indeed providing unique guidances for 3D tokamak design, optimization, and control.

Keywords 3D fields · Magnetic islands · Edge-localized modes · Tokamak control

1 Introduction and background

A tokamak strongly relies on the axisymmetry in the magnetic field to confine hot charged particles while remaining sensitive to a non-axisymmetric (3D) magnetic perturbation (Boozer 2008, 2010; Helander et al. 2012). A non-axisymmetry as small as $0.01 - 0.1\%$ can even cause a disruption as well as substantial performance degradation, and thus any unexpected 3D error field (EF) in a tokamak requires proper correction algorithms (La Haye et al. 1992; Fishpool and Haynes 1994; Buttery et al. 1999; Scoville and LaHaye 2003; Park et al. 2007; Menard et al. 2010; Paz-Soldan et al. 2014; In et al. 2017). This sensitivity, on the other hand, also leaves powerful utility of 3D fields, as has been highlighted by the suppression of the edge-localized mode (ELM) crashes via a resonant magnetic perturbation (RMP) (Evans et al. 2004, 2006, 2008; Liang et al. 2007; Suttrop et al. 2011; Kirk et al. 2012; Jeon 2012; Nazikian et al. 2015; Sun et al. 2016). RMP ELM suppression and EF control indeed represent the two main apposing consequences of 3D fields (Park et al. 2018)—invaluable benefits on the profile and instability control but mostly at the expense of confinement degradation—which pose great challenges in developing 3D tokamak scenarios.

3D tokamak scenarios have become of great interest due to their potentials to maintain the high confinement mode (H-mode) (Wagner et al. 1984) but without ELMs. ELM crashes are otherwise almost inevitable in H-modes. As well known in tokamak science (Zohm 1996; Connor 1998; Snyder et al. 2007), ELM crashes are repetitive energy losses when the self-organized pressure gradient near the edge pedestal in H-modes, $\vec{\nabla} p_{ped}$, becomes steep enough to trigger local magnetohydrodynamic (MHD) peeling–ballooning instabilities. These ELMs can cause unrepairable damage to plasma facing components such as divertors and, thus, must be controlled in a reactor scale tokamak (Hawryluk et al. 2009). The possibilities of controlling ELMs using 3D fields were seen in early device experiments such as COMPASS-C (Hender et al. 1992) and JFT-2 M (Shoji et al. 1992) as summarized well in the early review paper (Evans 2015). Then, the full control of ELMs in the collisionality conditions projectable to the next-step devices has been demonstrated at the DIII-D tokamak from the year of 2003, by Evans et al. (2004) and his colleagues as documented by their seminal papers (Moyer et al. 2005; Evans et al. 2005, 2006, 2008; Fenstermacher et al. 2008). It was followed by the JET (Liang et al. 2007) and ASDEX-U (Suttrop et al. 2011) tokamaks as well as by the MAST spherical torus (Kirk et al. 2010) where ELM mitigations were achieved, and then the two superconducting tokamaks, KSTAR (Jeon 2012) and EAST (Sun et al. 2016), joined the group in early 2010s by fully suppressing ELMs with their flexible set of ELM control coils. These broadly validated applicabilities lead to the proposal of 3D fields as a primary scheme for ELM-free H-mode scenarios in the next-step devices such as ITER (Schaffer et al. 2008; Loarte et al. 2014).

Experimental evidences across the world program, however, are also regularly revealing seemingly inconsistencies. The early criteria based on the vacuum island overlap width (VIOW) developed over extensive DIII-D data (Fenstermacher

et al. 2008) were not always consistent with observations in other tokamaks (Kirk et al. 2015; Paz-Soldan et al. 2015; Park et al. 2018), or other operational regimes even in the same device, e.g., when the density is too high (Suttrop et al. 2018) or rotation is too slow (Moyer et al. 2017; Paz-Soldan et al. 2019), or the plasma shape becomes distinct (Nazikian et al. 2016). In particular, ELM suppression or acceptably strong ELM mitigation by 3D fields were never achieved in the spherical torus (ST) devices (Canik et al. 2009; Kirk et al. 2013) or even in the conventional tokamaks when the plasma shape becomes up-down symmetric (Hudson et al. 2010; Shafer et al. 2021). A number of important progresses have been made along with advanced diagnostics (Moyer et al. 2005; McKee et al. 2013; Wade et al. 2015; Nazikian et al. 2015; Lee et al. 2016; Choi et al. 2017; Ida et al. 2018; Park et al. 2022), and first-principle kinetic or MHD simulations (Park et al. 2010; Bécoulet et al. 2014; Waltz and Ferraro 2015; Orain et al. 2017; Kwon et al. 2018; Kim et al. 2020; Hager et al. 2020), but none to dates has been able to offer a universal predictability across those diversified phenomena. This paper is not intended to cover them all nor give comprehensive review of rich 3D field physics which can be rather found in other preceding review papers (Boozer 2010; Callen 2011; Wade et al. 2015; Evans 2015). This paper instead will focus on a brief review of a particular framework that has been successfully used particularly in the low-toroidal-mode (low-n) RMP ELM control in KSTAR, while still broadly aiming at developing common 3D physics basis and predictive schemes readily available for ELM control.

The rest of the paper is organized as follows. The framework along with perturbed 3D physics models in hierarchy will be summarized in Sect. 2 along with the hypothetical breakdown of physics basis. The following Sect. 3 will introduce recent evidences indicating that the 3D field coupling is well separable from complex resonant boundary layer dynamics. Section 4 will introduce important progress on the resonant layer modeling, which has been greatly improved in last decade as validated over several definitive features of RMP ELM suppression such as q_{95} window. Transport under 3D fields can take place in various channels, some of which require knowledge beyond MHD or across non-confined boundary region, as will be discussed in Sect. 5 on the selected topics such as momentum transport or heat fluxes to the divertors. Section 6 will show recent advances on the real-time 3D field control which finds an optimal trade-off between stability and confinement, and also on the 3D coil designs under the adopted framework. Then this paper will be concluded with brief summary and remarks for future work.

2 3D field physics basis and hypothesis

2.1 Classification of 3D fields

3D fields in tokamak science are often mixed in use and confusing. Precisely, a 3D field in a tokamak only means a small non-axisymmetric magnetic perturbation $\delta\vec{B}$ compared to the main tokamak magnetic field $\vec{B}_0$. Thus, a 3D field cannot alter the fundamental nature of tokamak confinement, such as that toroidal plasma currents

must be induced to provide a rotational transform. However, the radial component contained in the perturbation $(\delta\vec{B} \cdot \hat{n})$ to the $(\vec{B}_0 \cdot \hat{n}) = 0$ surfaces can strongly distort tokamak plasmas even with $|\delta\vec{B}|/|\vec{B}_0| = 10^{-3} \sim 10^{-4}$, by inducing magnetic islands in a significant fraction of plasma volume. "3D" field in a tokamak is a terminology adopted to emphasize such a powerful impact, and also to comprehend a diversity of magnetic perturbations more than RMPs. A RMP can also be an ambiguous term in toroidal plasmas where it is not easy to isolate a resonant part of a magnetic perturbation $\delta\vec{B}_{mn}$. Here, m is the poloidal and n is the toroidal harmonic number, which can resonate at a surface where magnetic field lines have the identical helical pitch, $q = m/n$. Strong poloidal mode coupling exists almost always unless the plasma shape is circular in a very large aspect ratio $A = R/a \to \infty$, where R is the major radius and a is the minor radius of a torus. Toroidal mode coupling can also occur non-linearly when the perturbation becomes locally sizable. In fact, most of the 3D fields tested in tokamaks contain non-resonant contents as much as resonant contents in terms of their amplitudes in vacuum space. It is the plasma response that amplifies resonant (Boozer 2001), or near-resonant components (Lanctot et al. 2010, 2011), supporting the logic to treat any 3D field as a RMP to the leading order. Nonetheless, it is still useful to classify 3D fields in the following three categories.

- RMP (resonant magnetic perturbation) (Evans et al. 2004):
  3D field containing significant (m, n) components which can resonate with unperturbed plasma on the $q = m/n$ rational surfaces, somewhere in the core or the edge, and possibly break the surfaces into magnetic islands by "field penetration" (Fitzpatrick and Hender 1991; Fitzpatrick 1993; Fitzpatrick 2004; Fitzpatrick and Waelbroeck 2005; Cole and Fitzpatrick 2006; Cole et al. 2008; Fitzpatrick and Waelbroeck 2008, 2009; Fitzpatrick 2016; Fitzpatrick 2018a, b).
- NRMP (non-resonant magnetic perturbation) (Park et al. 2013):
  3D field not containing any impactful resonant components even after plasma response, but having components $(m \pm \Delta m, n \pm \Delta n)$ that can induce strong transport globally across deformed surfaces. The signature phenomenon is the rotational damping by "neoclassical toroidal viscosity (NTV)" (Shaing 1983, 2003; Shaing et al. 2008; Zhu et al. 2006; Park et al. 2009; Sun et al. 2010, 2012; Shaing et al. 2015).
- QSMP (quasi-symmetric magnetic perturbation) (Park et al. 2021):
  3D field minimizing the variation in the field strength along the field lines. The field lines must be perturbed field lines since the field strength along the actual particle trajectory, i.e., "Lagrangian" field strength δB_{Lmn} (Boozer 2006; Park et al. 2009) is what determines transport of guiding-center plasmas. As a result, it is not accompanied either by field penetration or NTV, even if magnetic perturbations are large in amplitudes.

Note that RMP or NRMP is identifiable only by local field line geometries, at least conceptually, but QSMP requires the estimation of perturbed field lines in 3D equilibrium or often the kinetic particle trajectories to minimize the effects of transport as it is not normally possible to achieve $\delta B_{Lmn} \to 0$ everywhere. Still QSMP is a mutually exclusive group of fields as there are no RMP or NRMP

effects, by the definition, despite its large amplitude of perturbations. The possibility to form such a perturbation has been demonstrated recently in KSTAR and DIII-D (Park et al. 2021) and thus it deserves a distinct category in the 3D optimization.

Optimizing 3D fields should comprehend all above, but in this paper will mean optimizing only RMPs which create the leading-order effects in tokamaks through plasma response. NRMP effects encapsulated by NTV will be considered as a side, or subsidiary effect, to be optimized for the next order as needed. Note that NTV is not only driven by NRMPs, but also by RMPs especially near magnetic islands (Shaing 2001; Kim et al. 2013) and can play an important role in establishing transport required for ELM suppression. Therefore, RMP optimization will also lead to NTV optimization to some extent, although those two are not necessarily correlated linearly.

2.2 Hypothesis on RMP responses—bifurcations of 3D tokamak equilibria

A key hypothesis to understand resonant tokamak responses is that it is the bifurcation among perturbed equilibria that leads to an ELM-free state from an ELMying state. The bifurcation refers to the process known as the resonant field penetration, or equivalently the opening process of magnetic islands at the resonant surfaces (Fitzpatrick and Hender 1991; Fitzpatrick 1993; Fitzpatrick 2004; Fitzpatrick and Waelbroeck 2005; Cole and Fitzpatrick 2006; Cole et al. 2008; Fitzpatrick and Waelbroeck 2008, 2009; Fitzpatrick 2016; Fitzpatrick 2018a, b). This process is non-ideal and non-linear, establishing a dynamic path between pre- and post-ideal MHD equilibria in the presence of 3D fields. In addition, this process is assumed to be sufficiently local around the resonant surfaces which are valid as long as the size of magnetic islands remains small, as it does especially before the full field penetration. This hypothesis is followed by further breakdown;

(I)   *Before the field penetration*:

   Entire plasma evolves ideally and initially establishes resonant coupling, in between Alfven τ_A and sound τ_s time scales, along with screening parallel currents $j_\parallel$ at each resonant layer to preserve magnetic topology (Boozer 2004; Park et al. 2007; Bécoulet et al. 2012; Waelbroeck et al. 2012). Optimizations of 3D field spectrum for resonant coupling can therefore be approximated reasonably well with ideal perturbed equilibria. See Sect. 3.

(II) *After the field penetration*:

   If the screening parallel current or an implied resonant field at a particular surface reaches a threshold, the resonant field, or the resonant helical flux ψ_{mn} (Fitzpatrick and Hender 1991; Park et al. 2008), penetrates and opens magnetic islands rapidly until non-linearly saturated, in later non-ideal time scales such as resistive τ_r or viscous τ_v time scales (Fitzpatrick 2012). Its immediate consequence depends on the location of resonant surfaces where the field penetration takes place.

(i)   If the field penetration occurs at a core low (m, n), particularly (2, 1) or (3, 2), surfaces, born-locked islands become big enough to disrupt entire plasma (La Haye et al. 1992; Fishpool and Haynes 1994; Lanctot et al. 2017; Hu et al. 2020).

(ii)   If the field penetration occurs at the innermost edge, or at the top of the pedestal, the saturated islands are only big enough to reduce the pedestal height closely to ELM instability boundary. This hypothesis has been used successfully in theory and modeling (Waelbroeck et al. 2012; Hu et al. 2020a), but also backed up by several observations including synthetic diagnostics (Nazikian et al. 2015; Choi et al. 2022; Willensdorfer et al. 2022) although it is still challenging to directly measure the small edge islands.

(iii)   If the field penetration occurs at the outermost edge region, or at the foot of the pedestal, no direct change in MHD instabilities is expected but substantial particle transport such as density pump-out may still occur (Hu et al. 2019, 2020b). See Sect. 4.

(III)   *Transport during ELM suppression*:

Non-linear island evolutions during ELM suppression are accompanied with changes in transport relevant for guiding-center plasmas. Transport here includes $\vec{E} \times \vec{B}$ convection associated with ion polarization currents inside islands (Hu et al. 2019, 2020a) and neoclassical diffusion due to wobbled magnetic surfaces (Liu et al. 2017), but not anomalous turbulence. This means to assume anomalous transport coefficients such as viscosity and thermal diffusivity same throughout the field penetration. See Sect. 5.

(IV)   *Transport after ELM suppression*:

NTV by NRMPs or heat flux to the region outside plasma will be assumed to be only a consequence by ELM-suppressed states rather than intervening effects. Optimizing these two in particular, under ELM suppression, are indeed important subjects. Rotational damping by NTV as a result of RMP applications can change various other instabilities. Resulting steady heat flux to the divertors would also better be minimized while ELM suppression should be maintained to avoid transient heat flux (Hawryluk et al. 2009; Loarte et al. 2014; In et al. 2017). Changes of anomalous transport in new magnetic topologies, in comparable or different time scales (Ida et al. 2018; Ishizawa et al. 2019; Taimourzadeh et al. 2019; Hager et al. 2020; Hahm et al. 2021), are beyond the scope of this paper and so will be discussed only briefly. See also Sect. 5.

Note also in the cases of (II.ii)–(II.iii), magnetic islands are sufficiently local and, thus, ideal MHD can still dominate globally in outer layers which can be used to match layer solutions, or even as an approximation for entire plasma region after taking the modified 2D profiles when modeling (IV) transport physics after ELM suppression. These presumptions have been tested in recent experiments especially in KSTAR as will be reviewed in the following sections.

3 Optimizing 3D field spectrum for ELM suppression

Many degrees of freedom in 3D space is indeed the central complexity in 3D field optimizations. Device-to-device variations in coil row position and shape easily confuse studies and their interpretations without a clear physics basis, as illustrated in Fig. 1 for examples. (a) DIII-D has the 1×6 ex-vessel coils at the midplane called C-coil which are mostly used for EF control and also the 2×6 in-vessel coils at the off-midplane called I-coils that are used for both EF and ELM control (Luxon et al. 2003). (b) NSTX has the 1×6 midplane coils which are ex-vessel although they are as close as other in-vessel coils (Bell et al. 2006). The in-vessel 2×12 non-axisymmetric control coils (NCCs) are only conceptual for NSTX-U in the future as studied for the purpose of ELM control when desired (Lazerson et al. 2015). (c) COMPASS is equipped uniquely with the 2×4 high-field-side (HFS) coils as well as other low-field-side (LFS) coils (Markovic et al. 2018). (d) KSTAR is also unique in having the 3×4 in-vessel coils at the midplane as well as at the off-midplane (Lee 2000). (e) ITER is planning to have the most complicated 3D coil set including the 3×6 ex-vessel coils for EF control and the 3×9 in-vessel coils for ELM control (Schaffer et al. 2008).

Even in a single device, a question can remain on whether or not unexplored 3D fields could provide better access to or reliability for ELM suppression. This was a situation in KSTAR, where there are 3 rows of coils near the top, midplane, and bottom as shown in Fig. 1d, each of which can be independently controlled for the amplitude and also the phase of $n = 1$ perturbations. Note under linear response, the toroidal mode n's are not coupled since a tokamak before perturbation is axisymmetric (i.e., $n = 0$). KSTAR has shown the complete ELM suppressions
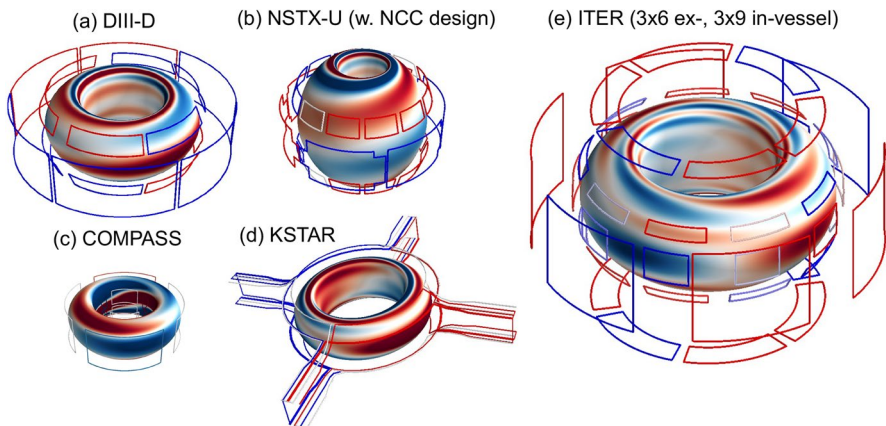

Fig. 1 Examples of various 3D coils. **a** 1×6 ex-vessel midplane coils and 2×6 in-vessel off-midplane coils in DIII-D. **b** 1×6 ex-vessel midplane with conceptual 2×12 in-vessel off-midplane coils in NSTX-U. **c** 2×4 in-vessel high-field-side (HFS) coils and 1×4 in-vessel midplane coils in COMPASS. **d** 3×4 in-vessel midplane and off-midplane coils in KSTAR. **e** 3×6 ex-vessel coils and 3×9 in-vessel coils at the midplane and off-midplane planned for ITER. Each contour on the plasma boundary surface illustrates the helical variations of 3D magnetic fields normal to the surface due to plasma response

using $n = 1$ in many discharges since its first demonstration in 2011 (Jeon 2012), but using almost one exclusive RMP configuration called standard 90° phasing. This configuration is characterized by $I = I_T = I_M = I_B$, i.e., the same $n = 1$ currents at the top, midplane, bottom coils respectively and also by $\phi_{TM} = \phi_{MB}$ which means the same phase differential between the top-to-midplane and the midplane-to-bottom. The standard 90° phasing represents only a single operating point in five-dimensional coil phase space.

It is practically impossible to test all 3D field options conceivably in five-dimensional coil phase space. Then, the predict-first experiments took place in 2016, using ideal perturbed equilibrium simulations based on the (I) presumption. By taking also the assumptions for (II.i) and (II.ii) qualitatively but empirically taking the field penetration thresholds for the core and the edge near the top pedestal, δB_{cT} and δB_{eT}, from a single operating point with the standard 90 ° phasing. Then by evaluating those core and edge resonant fields as a function of 5 coil variables, i.e., $\delta B_{c,e}(I_T, I_M, I_B, \phi_{TM}, \phi_{MB})$, from ideal perturbed equilibria, it became possible to visualize the entire map of ELM suppression windows in the coil space based on $\delta B_c < \delta B_{cT}$ since otherwise it means locking (II.i), and $\delta B_e > \delta B_{eT}$ for ELM suppression as otherwise it means no MHD instability change (II.ii).

The diagram in Fig. 2 shows those three possibilities, locking (red), no instability change with non-resonant response only (green), and ELM suppression (blue), in the case with the maximum currents at the top and bottom coils $I_T = I_B = 5kA$, as a function of remaining variable $(I_M, \phi = \phi_{TM} = \phi_{MB})$. This subspace was never explored before 2016 but was particularly chosen since there is the second ELM
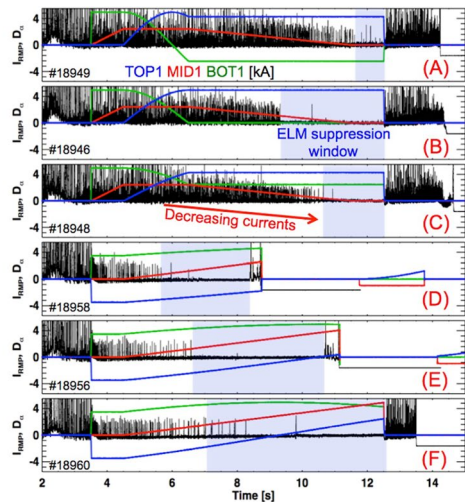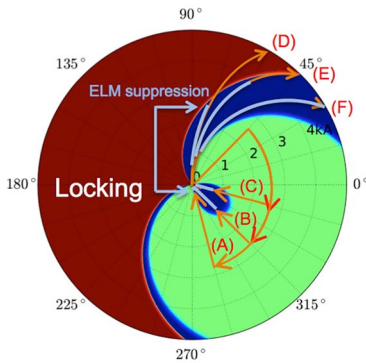

Fig. 2 Stability diagram on the left with $n = 1$ RMP as a function of $(I_M, \phi = \phi_{TM} = \phi_{MB})$ with $I_T = I_B = 5kA$ predicted for a KSTAR 2017 target plasma. The (**A–F**) orange curves show the experimentally tested variations and the overlaid light blue sections in the curves are the validated ELM suppression windows, as followed by time traces of D_α and coil currents for each (**A–F**) case on the right. Figure is taken and modified from Ref. Park et al. (2022). More details for the predicted diagram, coil phase space and experimental traces can be found in Ref. Park et al. (2018)

suppression window accessible only by dynamic 3D field variations, as illustrated in the (A–C) paths. The (A–F) trajectories in Fig. 2 show the experimentally tested variations of (I_M, ϕ) based on the prediction, which indeed validated the predicted ELM suppression windows in every path as highlighted by overlaid light blue curves. Note that similar results were already obtained in 2016 as published in Park et al. (2018) but here the results in 2017 covered more complex variations of 3D coils for new target plasmas to extend the validations (Park et al. 2022).

These results demonstrate that the variable effects due to 3D field spectrum can be predicted by linear and ideal MHD response to 3D fields, consistent with the (I) assumption. Machine–machine variations of 3D coils are no longer confusing once the resonant fields at the core and edge (here in average sense) are identified. Also, the results show that the outer-layer coupling between 3D coils and resonant fields is well separable from the field penetration process in layer. In particular, the field penetration thresholds for core and edge are shown to be independent of the variations in 3D fields as assumed, since otherwise the ELM suppression windows would not have been predicted with the fixed thresholds. The degree of 3D variability in KSTAR is large enough for one to generally claim the validity of these assumptions in entire 3D field space.

4 Understanding parametric accessibility and dependencies of RMP ELM suppression

The variability of 3D field spectrum is predictable reasonably well with ideal perturbed equilibria as described in Sect. 3, but the actual operating windows for ELM suppression shown in Fig. 2 can be identified only when the threshold conditions for the core and edge are known. By following the (II) assumption, one needs to understand the field penetration process near the resonant surfaces. There is no fundamental difference in the field penetration physics (Waelbroeck et al. 2012; Fitzpatrick 2018a; Hu et al. 2019, 2020) among different resonant surfaces as long as the magnetic islands are small and local, which is always true at least initially till the onset of the field penetration. Recent modeling by the non-linear two-fluid MHD code called TM1 (Yu et al. 2008; Hu et al. 2019, 2020, 2020b, 2021a) indeed shows the similar parametric dependencies of the threshold conditions for the core $(m, n) = (3, 2)$ locked modes (LMs) (published in Ref. Hu et al. (2020)) and for the edge $(m, n) = (5, 1)$ ELM suppression as

$$\delta B_{32}/B_t \propto n_e^{0.56} T_e^{0.6} B_T^{-1.15} \omega \quad \text{(DIII-D, LMs)}, \tag{1}$$

$$\delta B_{51}/B_t \propto n_e^{0.62} T_e^{0.6} B_T^{-1.05} \omega_E \quad \text{(KSTAR, ELM suppression)}, \tag{2}$$

where n_e is the electron density, T_e is the electron temperature, ω is the toroidal rotation, ω_E is the $\vec{E} \times \vec{B}$ rotation, each at the rational surfaces, and B_T is the toroidal field at the magnetic axis. Figure 3 shows the examples of those TM1 simulations, using and scaling the profiles measured from a ELM-suppressed discharge with the
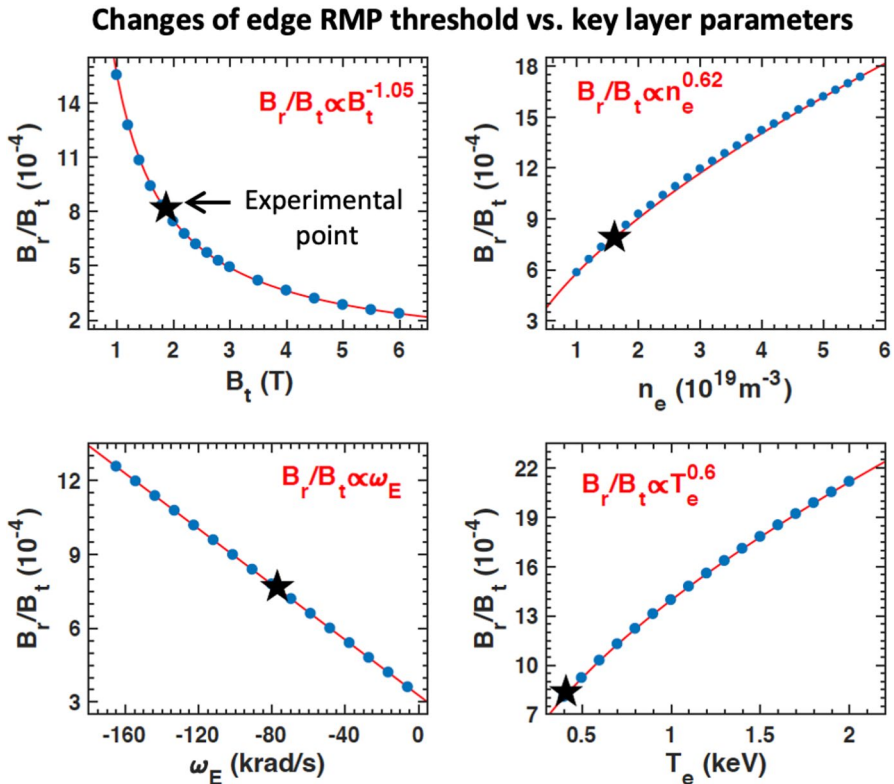
Changes of edge RMP threshold vs. key layer parameters

Fig. 3 TM1 predictions of parametric dependencies and scaling of the (5, 1) field penetration in the edge, with scaled profiles measured from a KSTAR discharge #18730. Electron density (n_e), $\vec{E} \times \vec{B}$ rotation (ω_E), and electron temperature (T_e) are local at the (5, 1) rational surface, but the toroidal field B_t is the value at the magnetic axis

$n = 1$ RMP in KSTAR. Note in the comparison that the rotational dependencies are represented differently by ω vs. ω_E for the core vs. edge. This difference is ignorable for the core but not in the edge where the diamagnetic flows by each species or neoclassical poloidal flow have rapid variations so as to comprise toroidal rotation in balance quite differently from $\vec{E} \times \vec{B}$ rotation. In more detail, it is known that the critical rotation for RMP ELM suppression may be neither ω or ω_E, but the one with an offset by ion or electron diamagnetic flow (Fitzpatrick 2018a; Paz-Soldan et al. 2019; Hu et al. 2020a). All these indicate the complexity of the edge profiles by which the ELM suppression phenomena appear to be richer than the core LM phenomena.

The parametric scaling shown in Eqs. (1–2) may look odd as there are scale-dependent parameters. It is largely motivated by strong correlations seen empirically with operational conditions such as electron density, particularly for the core LMs (Fitzpatrick 2012; Logan et al. 2020). It is shown that the parametric scaling can be reformed into non-dimensional physical parameters with additional parameters

such as the plasma size (Connor and Hastie 1973; Wolfe et al. 2005), but the operational parametric scaling is currently offering the best predictive measure. Still, the empirical scaling is not always seen consistent with the numerical scaling since even the operational parameters cannot be completely isolated in experiments. For example, empirical scaling for the core LMs due to error fields (EFs) tend to pronounce the density dependency much more than the temperature dependency. This led to the error field correction strategy to follow mainly the empirical threshold scaling developments based on tokamak database (Buttery et al. 1999; Logan et al. 2020; Hu et al. 2020), while using the numerical scaling as a guidance and also to understand the inter-parametric dependencies (Hu et al. 2020).

It is important to note that the local δB_{32} or δB_{51} are matching points to the ideal outer-layer solutions in a layer modeling. TM1 simulations are not exactly local as it covers the entire plasma domain but match the fields at the plasma boundary which is not an unreasonable assumption for RMP ELM suppression as the edge resonant surfaces are close to the boundary surface. This separation of the inner non-ideal and outer ideal layers via asymptotic matching is the key to error field threshold scaling to avoid LMs and can also be taken as a compelling approach to predict RMP ELM suppression in our framework. One of the recent highlights is the prediction of q_{95} windows for RMP ELM suppression and validation across the entire KSTAR database shown in Fig. 4. These impressive results were published already in Ref. Hu et al. (2021b) but Fig. 4 includes additional data points collected during the 2020–2021 KSTAR experimental campaigns.

The so-called q_{95} window has been known for the most characterizing feature of RMP ELM suppression since it was first reported by Todd Evans (Evans et al. 2008). As q_{95} represents the helical pitch for the main field lines in the edge, it is indicative to the resonance required between the main field lines and applied perturbations in the edge. Nonetheless, it was difficult to quantitatively explain the steep changes of RMP ELM suppression along with the edge q conditions. RMP ELM suppression appears to be even almost impossible when the q_{95} is not carefully adjusted although there are several resonant surfaces that can cover the edge region by one to another when q_{95} changes. It turns out that the location of the resonant surface needs to be close enough for the location of stationary flow and also for the location of the top of pedestal so that the particle transport can become strong enough to reduce the pedestal and change the ELM instability (Hu et al. 2019; Paz-Soldan et al. 2019). These conditions can meet only in a narrow q_{95} window as were shown quantitatively for the first time by TM1 simulations. One can see from Fig. 4 the steep changes of pedestal pressure degradation along with q_{95}, which will appear as a q_{95} window given a fixed RMP current. The condition matching is repeated roughly when one rational surface replaces another at the same location, establishing good n windows per the unit change of q_{95}. These results are overall consistent with the KSTAR observations in many years as can be seen by the overlaid data points. Note that TM1 simulations can not predict whether or not the predicted pedestal change can actually lead to ELM stability change and so here assumed 15% degradation as requirements to achieve ELM suppression.

The condition like q_{95} can be categorized as an accessibility condition, in addition to threshold conditions, e.g., Eqs (1–2), as ELM suppression becomes almost
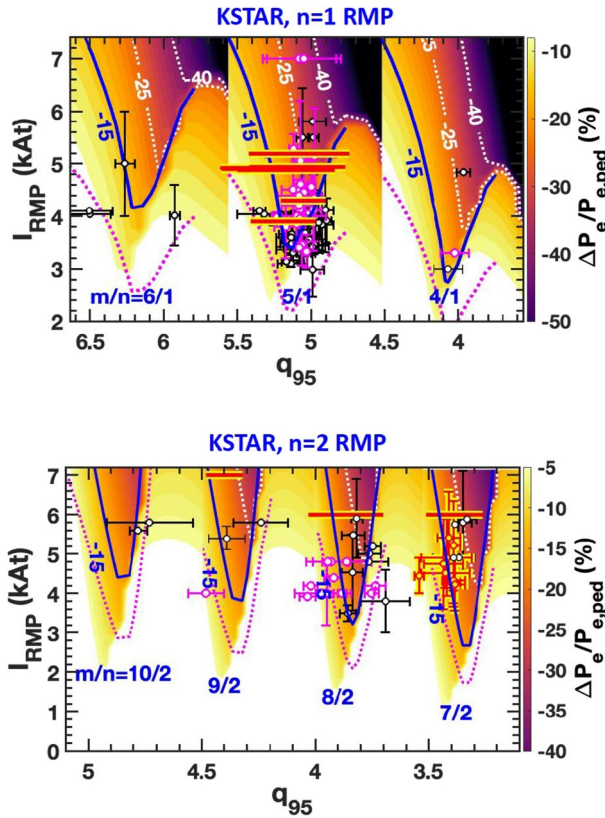
Fig. 4 q_{95} windows for RMP ELM suppression in KSTAR predicted by the TM1 code, retrieved from Fig. 8 in Ref. Hu et al. (2021b) and updated with new data obtained in 2020 and 2021 KSTAR campaigns. The contour indicates the predicted pedestal pressure modification due to $n = 1$ (Top) and $n = 2$ (Bottom) RMP currents as a function of q_{95}. Thick blue lines indicate where 15% reduction of the pedestal pressure is reached as assumed for the boundary of ELM suppression window. Threshold data obtained in KSTAR experiments are overlaid by points or bars, explaining the favorable q_{95} conditions for ELM suppression seen many years in KSTAR

inaccessible out of a narrow conditional window. Another such example is the plasma shape condition. RMP ELM suppression was never observed in the up–down symmetric double-null configuration (Hudson et al. 2010; Shafer et al. 2021; Liu et al. 2021), and becomes very difficult even in a single-null configuration when the triangularity becomes too high (Suttrop et al. 2017; Paz-Soldan et al. 2019; In et al. 2019). It has been shown that these shape effects are partially due to the strong variation of 3D plasma response relative to the minor changes in the shape itself, especially in the high-field side (HFS) (Paz-Soldan et al. 2015). This was known for the double-null vs. single-null configurations but recently also shown for high-triangularity cases. As published in Ref. Gu et al. (2022) and validated, Fig. 5 shows
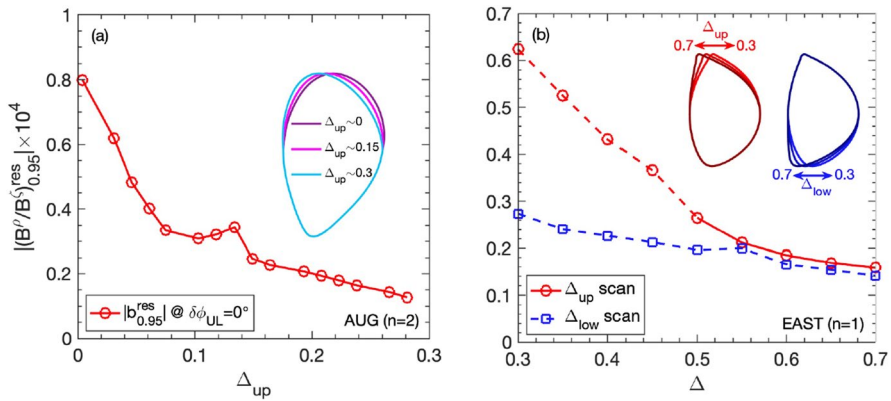
Fig. 5 Variations of 3D plasma response due to shape changes in **a** ASDEX-U and **b** EAST, as predicted by MARS-F simulations and validated by experiments. Figures are taken from Fig. 4 in Ref. Gu et al. (2022). The rapid decrease of plasma response for higher triangularity (Δ) implies the potential difficulties to generate strong enough response to suppress ELMs

the rapid changes of the HFS plasma response in the MARS-F modeling when the triangularity increases in each EAST and ASDEX-U target plasma. Note that the triangularity itself was changed in a significant range, but this change is very small compared to the shape as a whole.

The changes in plasma response due to shaping, however, do not seem enough to explain the steep changes of the accessibility to ELM suppression. Since the local layer would not see directly the shaping effect taking place in outer layers, a layer modeling alone is not expected to fill the gap here. There are possibilities to have significant changes in the edge profiles along with the boundary conditions near the primary plasma facing components, e.g., through the X-point changes along with the lower triangularity in the lower single-null (LSN) cases. However, the AUG experiments in Fig. 5a in Ref. Gu et al. (2022) with the upper triangularity scan with a LSN plasma are clearly against this idea. The shape accessibility conditions are not yet fully resolved after all, motivating more comprehensive modeling in full geometry, without approximating the dynamics separate across the resonant layers, perhaps also by integrating kinetic transport models.

5 Understanding underlying transport induced by 3D fields

3D responses including field penetration also change underlying particle, momentum, and heat transport. Toroidal momentum transport that creates rotational damping is almost always followed unless the applied field is quasi-symmetric (Nürenberg and Zille 1988; Boozer 1995), i.e., a QSMP (Park et al. 2021) in a tokamak. This well-known neoclassical toroidal viscous (NTV) process occurs even when the applied field is non-resonant, i.e., an NRMP through the non-axisymmetric surfaces (Shaing 1983, 2003; Shaing et al. 2008; Zhu et al. 2006; Park et al. 2009; Sun et al. 2010, 2012; Shaing et al. 2015). However, it is believed that NTV across

deformed surfaces alone, without modified magnetic topologies, is not strong enough to change thermal particle or heat transport which are already anomalously larger than neoclassical expectation. Only when the applied field is resonant enough to change the magnetic topologies, i.e., the RMP field penetration, a meaningful particle or heat transport may be followed altering the major pressure profiles and thereby instability.

The most characteristic transport phenomenon in the presence of RMPs is the so-called density pump-out (Evans et al. 2006, 2008). Assuming the quasi-neutrality, the plasma (electron) density n_e evolution can be represented by

$$
\frac{\partial n_e}{\partial t} + \vec{\nabla} \cdot \left[n_e (\vec{u}_E + \vec{u}_{e*} + \vec{u}_\parallel) \right]
$$
$$
= \frac{1}{e} \vec{\nabla} \cdot \vec{j}_\parallel + \vec{\nabla} \cdot \left[(D_\perp + D_{NA} + D_{NT}) \vec{\nabla} n_e \right] + S_n,
\tag{3}
$$

with a source S_n. The second part in the LHS is largely convective assuming the total flow $\vec{u} = \vec{u}_E + \vec{u}_{e*} + \vec{u}_\parallel$ with the $\vec{E} \times \vec{B}$ flow, the electron diamagnetic flow, the parallel flow, respectively, and is almost incompressible. The first part in the RHS represents the polarization effects due to electron quickly following the field lines in non-axisymmetric magnetic topologies. It is shown that the precise description of the polarization currents is the key to the simulation of density pump-out with isolated magnetic islands (Hu et al. 2019). The electric field associated with the polarization currents modifies $\vec{u}_E \propto \vec{E} \times \vec{B}$ which then convects the particles across flux surfaces inside magnetic islands. The second part in the RHS represents neoclassical and anomalous diffusive process. $D_\perp$ represents the cross-field diffusion mainly created by tokamak turbulence. D_{NA} (Park et al. 2009) is the non-ambipolar diffusion associated with non-axisymmetric variation in the field strength and NTV. The last D_{NT} reflects the potentially modified turbulent process due to magnetic islands or stochastic field lines.

The polarization currents evolving $\vec{E}$ upon non-axisymmetric perturbations and subsequent $\vec{E} \times \vec{B}$ convective transport across islands were explained first in detail by Rutherford et al. in Rutherford (1973). This classical transport appears to be the leading-order driver for density pump-out as well as the critical component to be self-consistent to reproduce the field penetration, as successfully shown recently by extensive TM1 simulations (Hu et al. 2019, 2020b, a, 2021a, b). Figure 6 shows the (a) evolution of magnetic islands at the (5, 1) rational surface due to RMPs and (b) the modified density profiles as a result from TM1 simulations, from the same KSTAR experimental case employed to find numerical threshold scaling in Fig. 3 and ELM suppression window in Fig. 4a. Figure 6a clearly shows a bifurcation process called the field penetration in the simulation when the (5, 1) RMP field increases from 12G to 14G, which then causes the density pump-out through the (5, 1) islands at the top of the pedestal and modifies the pedestal pressure profile strong enough to stabilize ELMs in KSTAR (Hu et al. 2021b).

This success may be somewhat a surprise since TM1, first of all, runs on a cylindrical geometry (Yu et al. 2008) even if it uses a full-geometry code GPEC (Park and Logan 2017) to specify the initial condition of 3D fields at the plasma
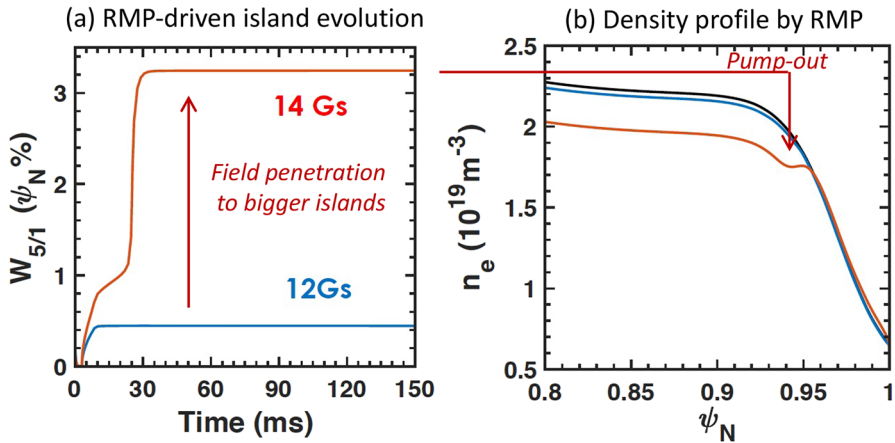
Fig. 6 TM1 simulations for the **a** evolution of (5, 1) magnetic islands in the two different amplitudes of RMP fields and **b** the modified electron density profiles as a result, clearly reproducing the field penetration and density pump-out process. The simulation is performed for the same KSTAR experimental case #18730 as one for Figs. 3 and 4a (Hu et al. 2021b)

boundary. An important implication is that the RMP-driven islands from the initially ideal responses remain still local to the leading order, as adopted by many analytic theories (Hazeltine et al. 1985; Fitzpatrick and Hender 1991; Fitzpatrick 1993; Waelbroeck 2003; Fitzpatrick 2004; Fitzpatrick and Waelbroeck 2005; Cole and Fitzpatrick 2006; Cole et al. 2008; Fitzpatrick and Waelbroeck 2008, 2009; Waelbroeck et al. 2012; Fitzpatrick 2016; Fitzpatrick 2018a, b) and consistent with (II) assumption in this paper. As extensively reported recently, in fact, TM1 demonstrated its predictive capabilities of RMP physics to many details in DIII-D and KSTAR. An example to the detail is the prediction for the staircase jump for the density pump-out (Hu et al. 2019, 2020a) since there are more than one rational surface each of which can bifurcate with bigger islands and the density pump-out. There are clear observations in DIII-D (Hu et al. 2019), EAST (Sun et al. 2016), and also recently KSTAR (*via private communication with S. K. Kim and Q. Hu*) supporting this idea. TM1 also explains that the density pump-out would occur almost always by RMPs even if ELMs are not suppressed, as happens in many cases, due to the field penetration at the outermost edge rational surfaces. These pictures are plausible as taken for (II.ii) and (II.iii) assumptions in Sect. 2 but yet to be validated in detail.

Second, TM1 runs with $D_{NA} = 0$ and $D_{NT} = 0$, i.e., no change in neoclassical or turbulent transport due to islands. This implies that these transport mechanisms may be subdominant over the classical mechanism implemented in TM1, which of course should be verified and validated with the full-geometry simulations. There are also other observations left unresolved yet. The difficulty to suppress ELMs in spherical torus devices was never clearly explained (Canik et al. 2009; Kirk et al. 2013). RMP ELM suppression was never achieved in the double-null divertor (DND)

configurations which appears to be only partially associated with the weak plasma response in the high-field-side (HFS) (Hudson et al. 2010; Shafer et al. 2021), again motivating the full-geometry simulations integrated with additional transport.

In toroidal geometry, magnetic islands are not equal in their shape at the resonant surfaces around the torus. Mode coupling, broadly speaking, can also come into play across Kink and tearing mode structure and also across different toroidal mode numbers non-linearly. Non-ambipolar transport, D_{NA}, is also an important toroidal effect as it is mainly driven by toroidally trapped particles. In fact, MARS simulations for MAST and DIII-D have shown that D_{NA} could be strong enough to cause substantial density pumping (Liu et al. 2017, 2020), as, therefore, taken here as the (III) assumption. These effects were all combined recently in the JOREK code (Bécoulet et al. 2012; Huijsmans and Loarte 2013; Kim et al. 2020), comprehensively unveiling their complex dynamics. JOREK runs on the full geometry non-linearly, and uses a reduced set of MHD equations, which has been recently updated in a way to have the polarization currents explicitly similar to TM1, and also now includes the D_{NA} effects using a semi-analytic formulation (Kim et al. 2021).

The integration of the semi-analytic D_{NA} calculations to a non-linear code deserves an explanation. Analytic formulations of D_{NA}, or equivalently neoclassical toroidal viscosity (NTV) transport (Shaing et al. 2015), are based on the well-defined flux surfaces with integrable field lines nested around the magnetic axis. When the field lines are not integrable, radial diffusive transport is no longer meaningful in neoclassical theory since the parallel transport can quickly overwhelm transport processes. However, if a 3D MHD code can still approximately yield surfaces confining plasmas, one can formulate extra diffusive process across the surfaces. Figure 7 shows the perturbed surfaces identified in JOREK by electron temperature with $\xi_\psi = \delta T_e/(dT_{e0}/d\psi)$ where ξ_ψ is the radial displacement of the surfaces, on
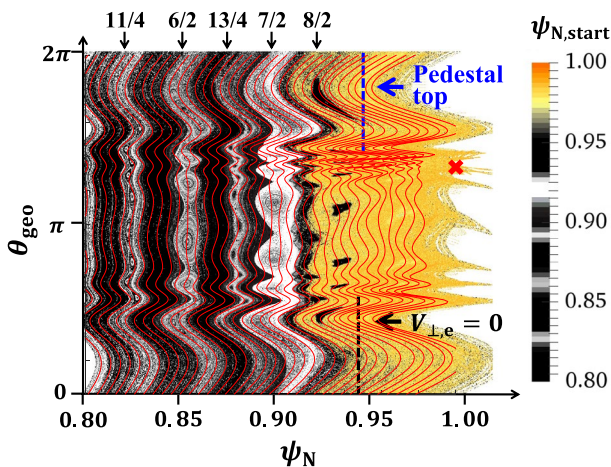

Fig. 7 Radial displacements of perturbed field lines identified by electron isothermal contours from non-linear JOREK simulation on a KSTAR $n = 2$ RMP discharge #18594. The underlying Poincare plot is taken from Fig. 10 in Kim et al. (2020), indicating the similarity and validity of the identifications

another KSTAR case where ELMs were suppressed by $n = 2$ RMP. One can see that the electron isothermal contour lines are consistent with the magnetic field lines from the view point of Poincare plot. Next step is to estimate the non-axisymmetric variation in the field strength that the particles see along their trajectories (Boozer 2006; Park et al. 2009; Logan et al. 2013). This requires additional kinetic information, which are the particle trajectories on the perturbed flux surfaces across the field lines. Here the approximation is to use ξ_α, fluid movements across the field lines on the surface, and to calculate ξ_α (Park and Logan 2017) based on ideal force balance assuming that ideal MHD dominates again once the islands or stochastic field lines are established.

By integrating the (ξ_ψ, ξ_α) structure identified from JOREK into the semi-analytic formulation implemented in a GPEC module, PENTRC (Logan et al. 2013), it was shown in Ref. Kim et al. (2021) that D_{NA} can indeed play an important role in toroidal geometry. In the $n = 2$ RMP case in KSTAR, the contribution from the neoclassical D_{NA} (or NTV) is shown to be comparable with one from the classical transport as shown in Fig. 8. This explained not only the observed density pump-out more successfully than the simulation without NTV, but also the observed rotation damping overall in terms of the total torque as reported by Kim et al. (2021). This kinetic-hybrid non-linear MHD simulation is relatively new and still under active developments, but generally it does show the complicated compensations across the neoclassical and classical mechanisms. For example, a strong near-resonant Kink structure can suppress islands and classical convective transport, but instead compensate the loss through the NTV associated with the Kink mode, as will be published in a separate paper.

In addition, potential modifications in anomalous transport across Kink, islands, or stochastic field lines, generally termed as D_{NT} here, should also be understood. Note that D_{NT} represents the direct changes of turbulence due to the
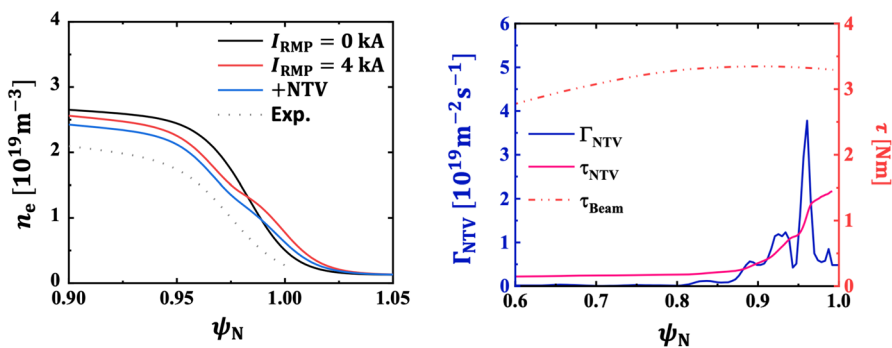

Fig. 8 Modified pedestal density profiles due to $n = 2$ RMP in the KSTAR discharge #18594, simulated in JOREK without (red) and with (blue) D_{NA}, or equivalently NTV, as shown at the figure on the left. D_{NA} appears to be essential to explain experimental data better as indicated in comparison to the experimental data (EXP). Simulated NTV particle flux (Γ_{NTV}), NTV torque (τ_{NTV}) compared to NBI injection torque (τ_{Beam}) profiles are also shown at the right. NTV total torque due to RMP is up to 31% of the beam total torque which roughly explains rotation damping observed in the experiment. Figures are taken and slightly updated from Fig. 2 in Kim et al. (2021)

3D structure, not the indirect changes due to modified 2D profiles such as $\vec{E} \times \vec{B}$ along the time. For example, recent gyrokinetic analysis (Hahm et al. 2021) and simulation (Taimourzadeh et al. 2019) indicate that vortex flows around magnetic islands increase turbulence along with spreading and, thus, radial transport across the X-points of island chains. These characteristics of turbulence around islands have been understood similarly in (neoclassical) tearing modes for years (Poli et al. 2009; Hornsby et al. 2015; Ishizawa et al. 2019) and recently became also of great interest in RMP topical areas. The gyrokinetic RMP simulations have been recently performed in KSTAR for further validations with the advanced imaging diagnostics, in a perturbative fashion using the 3D MHD solutions as a background and, thus, following the logic behind (IV) assumption.

The time scales of these classical, neoclassical, or turbulent transport due to 3D fields are not necessarily similar. The pedestal bifurcations with the field penetration in KSTAR have been well explained by non-linear MHD or neoclassical-hybrid MHD, but a gradual pedestal evolution later in time has also been observed in long pulses. This may be potentially due to a feedback between the same transport mechanisms and evolving profiles, but also possibly due to new transport such as turbulence in longer time scales. Note that all transport mechanisms with 3D fields can also significantly appear in thermal energy or heat channel (e.g., via non-ambipolar χ_{NA} or anomalous χ_{NT} thermal diffusivity). This paper focuses on particle channel, i.e., density pump-out, which appears to be most prominent, but underlying transport in heat channel should also be understood to predict temperature profiles under RMP ELM suppression.

Lastly, power flux into plasma facing components across or along the open-field lines is also a critical subject for transport resulted from 3D fields. Successful ELM suppression will remove transient heat flux to the divertors as desired, but can modify steady power fluxes in multiple ways. It can increase fast ion losses which can result in the increase of temperature for limiters and vessels (Bortolon et al. 2013; Van Zeeland et al. 2015; Xu et al. 2020), which can become a critical issue in long pulse as studied in KSTAR (Rhee et al. 2022). It can also increase steady flux to the divertors through the split strike points as discussed in many literature (Hawryluk et al. 2009; Jakubowski et al. 2009; Schmitz et al. 2011; Ahn et al. 2011; Harting et al. 2012; Loarte et al. 2014), or even the primary strike point as reported often in KSTAR (In et al. 2017, 2019). The prediction of heat flux to the divertors with 3D fields requires precise descriptions for the edge plasmas across the scrape-off layer (SOL) region including multi-species transport along the open-field lines and neutrals. The well-known EMC3-EIRENE code (Feng et al. 1997; Frerichs et al. 2010; Lore et al. 2017) can simulate these complex boundary phenomena given 3D MHD background solutions, again by following the (IV) assumption, as has been deployed across the international tokamak program.

Figure 9 shows an example of EMC3-EIRENE predictions in KSTAR, on the heat flux distribution at the outer divertor due to various $n = 1$ RMPs. Note that only the poloidal distribution is shown by taking the maximum heat flux along
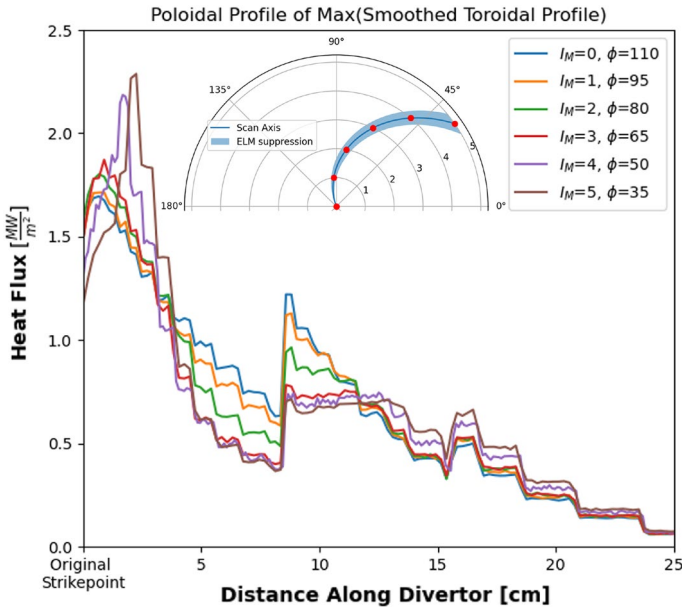
Fig. 9 On the courtesy of J. Blarcum and H. Frerichs. Heat flux profiles in the outer divertor simulated by EMC3-EIRENE on a KSTAR discharge #16586 as a function of 6 different $n = 1$ RMP operating points (red dot) under the (blue) ELM suppression window. The detail will be published by J. Blarcum et al. as a separate paper, but shortly here, the significant variations in the predicted heat flux profiles indicate the possibility to optimize heat flux while maintaining ELM suppression

the toroidal direction given each poloidal point on the outer divertor. The 6 RMP configurations shown in Fig. 9 are all under ELM suppression window for the studied target discharge #16586 as shown in blue on the 3D stability diagram. The 3D stability diagram is on the same coil space (I_M, ϕ) as the diagram introduced in Fig. 2 and is identical to Fig. 3 in Ref. Park et al. (2018). This new result in KSTAR indicates the possibility to meaningfully change and optimize heat flux on divertors while still maintaining ELM suppression, as will be published in more detail as a separate paper. For example, one of the currently important issues is to understand the dependencies of the predicted edge dynamics along the open-field lines including heat flux, on 3D MHD response solutions.

6 Controlling and designing 3D coils

The predictive capabilities for 3D field coupling in Sect. 3, parametric dependencies and accessibility conditions in Sect. 4, and transport in Sect. 5, can be used to optimize plasma scenarios and 3D fields. When a 3D field operating window exists with variable margins, it is the real-time control that can finally find an optimal operating point. Performance will degrade too much if 3D fields are excessive, but ELMs can crash if 3D fields are too marginal. So, it is a subtle trade-off which can
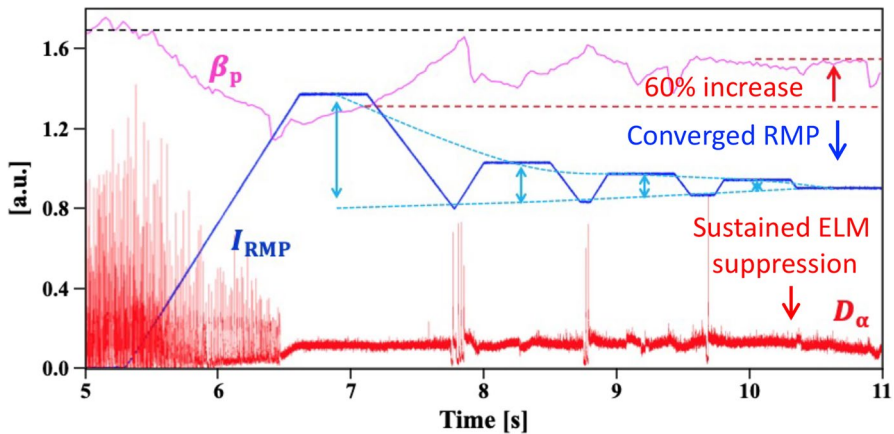
Fig. 10 An example of the adaptive $n = 1$ RMP control in KSTAR based on real-time D_α interpreters, minimizing confinement degradation (as shown by β_p parameter), while maintaining ELM suppression. The controller successfully converges to an optimal and stable operating point with up to 60% confinement restoration. Figure is taken from Fig. 1 in Kim et al. (2022) in a compact form

vary along the time especially in long pulse. Recently such a real-time ELM control has been successfully demonstrated through the KSTAR and Princeton University collaborations, using the real-time D_α detectors and adaptive 3D field controllers (Kim et al. 2022; Shousha et al. 2022). An excellent example is shown in Fig. 10 (Kim et al. 2022). Initially, RMP was increased until the detector found no ELMs. Then the controller decreased the RMP field to restore confinement as represented by β_p until the detector found ELMs back. Next cycles come with gradual improvements since the controller learned in what level the ELMs can be suppressed or not suppressed, toward the final convergence as established.

Note that the experiment above actually showed better performance than expected, due to unexpected gain during the control. As described in Kim et al. (2022) and as one can directly read from Fig. 10, the ELM suppression threshold became substantially different after the first cycle (after about 7.5 s). This is a surprise since the hysteresis was expected from non-linear simulations between the entering and exit point of ELM suppression, but not between the entering (or exit) points across different cycles. It turns out that a pedestal broadening mainly through ion channels was followed once ELMs were suppressed at the first cycle and then was sustained afterward even ELMs were back later during the feedback processes. The pedestal broadening then became beneficial by increasing edge resonant coupling, resulting in easier ELM suppression with lower RMP fields and thereby lower confinement degradation. This beneficial hysteresis appears to be associated with ion turbulent transport although it is not always accompanied depending on discharge conditions, motivating further research in this area. Also note that the ELM crashes needed by the detector to identify the lower bound may be not necessary if the detector can use the precursors in D_α baseline or other active spectroscopy which are under investigations in KSTAR.

The control margins or 3D field operating windows will be greater with more capable 3D coils (Logan et al. 2021). An important principle to follow in designing 3D coils for ELM suppression is the isolation of resonant coupling in the edge, relative to the core which is unnecessary. This optimizing principle (Park et al. 2018) is particularly critical for low-n RMPs since the core coupling can lead to the disruptive LM modes. The core resonant coupling for higher-n (> 2) may not lead to a disruption although it can still degrade performance unnecessarily. The high-n RMPs are, therefore, generally favored for ELM suppression as adopted for ITER, but their fast radial attenuation requires the 3D coils to be inside the vessel which will not be allowed for a reactor due to nuclear contamination.

The optimizing principle has been systematically implemented recently with GPEC, based on the new projection scheme to the core-null space (Yang et al. 2020). This scheme shows how a 3D field can be shaped in space to completely remove the core resonances while keeping the edge resonances. The so-called edge-localized RMP (ERMP) is characterized by curtailed perturbations near the outboard midplane as the core Kink mode is most amplified by perturbations near the outboard midplane. Its revealing characteristics offer an idea on how to design the coils in space as illustrated in Fig. 11 (Yang et al. 2020). By simply adjusting the existing window pane coils to roughly match the shape of the edge-localized RMP, ELM suppression windows can be largely expanded as a result of increased edge coupling relative to core coupling as shown in Fig. 11 (from (a) to (b)). More intelligent way of the coil design was also successfully tested, by integrating the
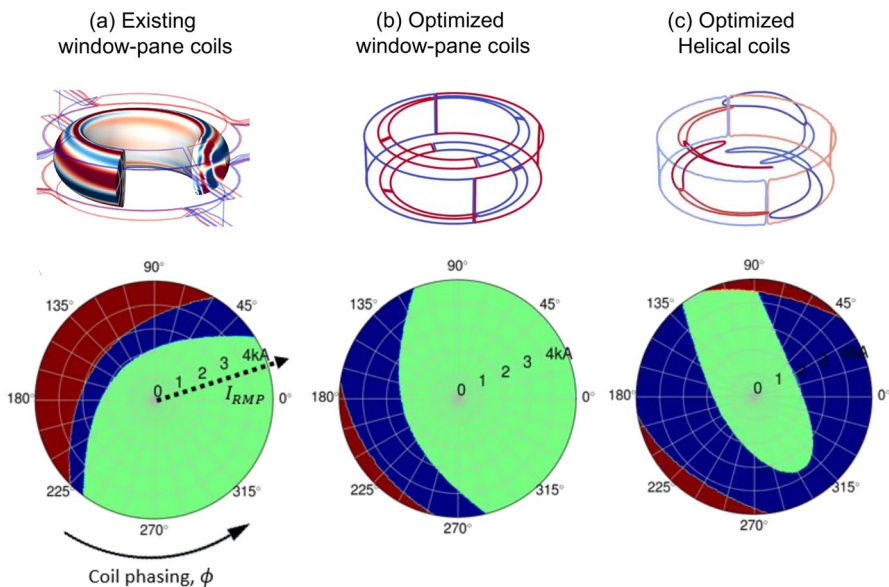

Fig. 11 Examples of optimized 3D coils designed for $n = 1$ ELM suppression on a KSTAR plasma. ELM suppression windows (in blue) are expanded when the window pane coils are adjusted based on the edge-localized RMP in (**b**) compared to (**a**), and even further when spacial adjustments beyond window pane shapes were allowed by FOCUS code in (**c**). Figure is taken from Figs. 8 and 9 in Yang et al. (2020)

optimizing scheme with 3D coil design tools. Figure 11c) shows that the 3D coils designed by a stellarator coil design code, FOCUS (Zhu et al. 2018), can indeed expand the ELM suppression even further than the simple window pane coils. Such a helical coil set may be less flexible in applications across different plasma scenarios, but this study indicates the possibility to find a highly optimized coil set for the baseline fusion plasma scenario using the low-n RMPs, by exploiting the large degrees of freedom to generate 3D fields.

7 Summary and concluding remarks

3D fields can offer a new and promising path to control transport and instabilities in tokamak scenarios but only when carefully optimized and controlled. Richness and complexities involved in 3D tokamak physics are manifested by the diversified observations across the world program. The attempts made here in this review are brief introductions to recent advances and remaining issues, along the particular framework taken by a collaborative group for KSTAR research to extend the predictive capabilities on 3D field ELM suppression. The framework is built on understanding of various types of 3D fields and inherently strong resonant tokamak responses, and on hypothesis of the local island bifurcation called field penetration as the central mechanism for ELM suppression through local profile modifications. The critical words are local bifurcation, enabling the reasonable separations of multi-scale in time and space for physics studies. An important example is the prediction of resonant coupling in entire 3D space using only ideal MHD equilibria as validated in KSTAR, allowing one to focus on local dynamics in common physics basis across the devices.

The prediction of the local bifurcation called field penetration is then required to identify actual 3D tokamak operational windows with suppressed ELMs. The parametric (or profile) dependencies can be separated to accessibility and threshold conditions. As shown and validated by pioneering TM1 work, the field penetration threshold depends strongly on local density, rotation, and B_T, as well known in the core locked mode bifurcation studies. This indicates no fundamental demarcation between the two bifurcations other than the differences in the profiles. The accessibility conditions are also critical as otherwise ELM suppression appears to be almost forbidden. TM1 applications show that one of the most well-known accessibility conditions, q_{95} window, is also predictable by non-linear two-fluid MHD, as validated over large KSTAR and DIII-D database. Other accessibility conditions such as shaping are yet to be resolved by perhaps more integrated simulations with transport, although recent studies indicate that the steep change of global 3D response may play an important role.

Understanding on transport mechanisms under RMP ELM suppression has also been greatly improved recently. The prominent density pump-out can be explained largely by convective $\vec{E} \times \vec{B}$ followed by ion polarization currents across islands, as shown by cylindrical TM1 applications. Nonetheless, toroidal effects such as mode coupling can complicate dynamics where neoclassical 3D transport or turbulence across islands and stochastic field lines can play important

roles. Recent JOREK simulations integrated with neoclassical toroidal viscosity (NTV) calculations indeed show the complex interplay between classical and neoclassical mechanisms as well as between Kink and tearing mode structures. Transport across and along the open-field lines is what determines power flux to plasma facing components during RMP ELM suppression after all. Recent applications of the cutting-edge EMC3-EIRENE 3D edge simulations indicate the possibility to optimize power flux under ELM suppression window, so as to minimize the steady heat flux as well as to remove transient heat flux.

Once the valid 3D field operational windows are identified, it is the real-time control that can find the best trade-off between stability and confinement. An excellent demonstration has been shown recently in KSTAR, using the adaptive 3D field control with the real-time D_α monitoring and by showing 60% confinement restoration when the feedback successfully converged. Benefits can be extended if 3D coils are designed to optimize the selective resonant coupling and to expand ELM suppression windows. A systematic optimizing scheme has been developed recently and adopted in KSTAR to optimize the configuration of existing coils as well as design innovative 3D coils for the future.

The framework here and its successful applications in the KSTAR tokamak as introduced in Secs. 3–6 look promising but will need to be tested further across the advanced regimes and devices. The importance of plasma response in RMP ELM suppression has been demonstrated widely across the devices (Paz-Soldan et al. 2015; Sun et al. 2016; Liu et al. 2017) other than the KSTAR, but it is not clearly demonstrated or quantified in high-n RMPs for which the plasma response tends to be suppressed. The hypothesis isolating local field penetration from global plasma response, and anomalous or open-field line transport from the field penetration process, is shown to work not only in the KSTAR $n = 1$ but also other RMP cases. For example, TM1 with its classical $\vec{E} \times \vec{B}$ convective transport and with GPEC global response could explain the dependencies on q_{95} and pedestal density in DIII-D for ELM suppression with $n = 2$ and $n = 3$ RMPs (Hu et al. 2019, 2020, 2021b). The prediction of heat flux, at least its splitting patterns, has been successful when the high-fidelity MHD solutions are used (Kirk et al. 2012; Nazikian et al. 2015; Lore et al. 2017; Orain et al. 2017; Kim et al. 2020), even without considering the changes in turbulence or potential feedback to the pedestal from the modified heat flux or Scrape-Off Layer (SOL) plasmas. Nonetheless, the hypothesis is still challenged by a number of RMP experimental results. As described in the Introduction, the inability or difficulties to achieve RMP ELM suppression in the up-down symmetric DND configuration, ST devices, high density or low rotation can be only partially explained by the combination of global plasma response and layer modeling, raising the concerns to extrapolate the results to entirely different regimes expected in ITER. The integration of the high-fidelity modeling can fill the gap as illustrated in the KSTAR studies but the improvements on the self-consistency across modeling will be required to understand and validate the predictabilities.

The real-time adaptive RMP control shown in the KSTAR should also be tested in other devices but its utility is quite clear for long-pulse next-step devices if 3D fields are chosen to control ELMs. As shown in Fig. 1e, ITER will have 27 dedicated in-vessel coils for ELM control which will be operated independently by 27 power

supplies. The flexibility to choose RMP spectrum with 27 knobs will be indeed unprecedented. It is, therefore, important to test how to utilize the flexibility in the optimization and real-time control in currently operating devices. For example, the integrated 3D modeling can tell us about the most reliable operating space of RMPs and then the real-time control can be preformed only within that pre-optimized operating space. In the future ITER experiments, it will also be important to exercise various RMP scenarios, e.g., not only the $n = 3$ or $n = 4$ as currently planned but also $n = 1$ and $n = 2$, to test its scientific feasibility in nuclear fusion reactors. The 3D optimization and feedback control will need to be integrated strongly with core 3D physics in those low-n scenarios, as illustrated by the KSTAR studies in this paper.

Data Availability The data that support the findings introduced in this paper will be available from the corresponding author, J.-K. Park and his co-authors, upon reasonable request.

Declarations

Conflict of interest The authors have no relevant financial or non-financial interests to disclose.

References

J.-W. Ahn, R. Maingi, J.M. Canik, A.G. McLean, J.D. Lore, J.-K. Park, V.A. Soukhanovskii, T.K. Gray, A.L. Roquemore, Effect of nonaxisymmetric magnetic perturbations on divertor heat and particle flux profiles in national spherical torus experiment. Phys. Plasmas **18**(5), 056108 (2011)

M. Bécoulet, F. Orain, P. Maget, N. Mellet, X. Garbet, E. Nardon, G.T.A. Huysmans, T. Casper, A. Loarte, P. Cahyna, A. Smolyakov, F.L. Waelbroeck, M. Schaffer, T. Evans, Y. Liang, O. Schmitz, M. Beurskens, V. Rozhansky, E. Kaveeva, Screening of resonant magnetic perturbations by flows in tokamaks. Nucl. Fusion **52**, 054003 (2012)

M. Bécoulet, F. Orain, G.T.A. Huijsmans, S. Pamela, P. Cahyna, M. Hoelzl, X. Garbet, E. Franck, E. Sonnendrücker, G. Dif-Pradalier, C. Passeron, G. Latu, J. Morales, E. Nardon, A. Fil, B. Nkonga,

A. Ratnani, V. Grandgirard, Mechanisms of edge localized mode mitigation by resonant magnetic perturbations. Phys. Rev. Lett. **113**, 115001 (2014)

M.G. Bell, R.E. Bell, D.A. Gates, S.M. Kaye, H. Kugel, B.P. LeBlanc, F.M. Levinton, R. Maingi, J.E. Menard, R. Raman, S.A. Sabbagh, D. Stutman, the NSTX team: New capabilities and results for the national spherical torus experiment. Nucl. Fusion **46**, 565 (2006)

A.H. Boozer, Quasi-helical symmetry in stellarators. Plasma Phys. Control. Fusion **37**, 103–117 (1995)

A.H. Boozer, Error field amplification and rotation damping in tokamak plasmas. Phys. Rev. Lett. **86**, 5059–5061 (2001)

A.H. Boozer, Physics of magnetically confined plasmas. Rev. Mod. Phys. **76**, 1071 (2004)

A.H. Boozer, Perturbation to the magnetic field strength. Phys. Plasmas **13**, 044501 (2006)

A.H. Boozer, Stellarators and the path from iter to demo. Plasma Phys. Control. Fusion **50**, 124005 (2008)

A.H. Boozer, Control of non-axisymmetric toroidal plasmas. Plasma Phys. Control. Fusion **52**, 104001 (2010)

A. Bortolon, W.W. Heidbrink, G.J. Kramer, J.-K. Park, E.D. Fredrickson, J.D. Lore, M. Podesta, Mitigation of alfven activity in a tokamak by externally applied static 3d fields. Phys. Rev. Lett. **110**, 265008 (2013)

R.J. Buttery, M.D. Benedetti, D.A. Gates, Y. Gribov, T.C. Hender, R.J. La Haye, P. Leahy, J.A. Leuer, A.W. Morris, A. Santagiustina, J.T. Scoville, B. J. D. Tubbing, the JET Team, the COMPASS-D Research Team, the DIII-D Team: Error field mode studies on jet, compass-d and diii-d, and implications for iter. Nucl. Fusion **39**, 1827–1835 (1999)

J.D. Callen, Effects of 3d magnetic perturbations on toroidal plasmas. Nucl. Fusion **51**, 094026 (2011)

J.M. Canik, R. Maingi, T.E. Evans, R.E. Bell, S.P. Gerhardt, B.P. LeBlanc, J. Manickam, J.E. Menard, T.H. Osborne, J.-K. Park, S.F. Paul, P.B. Snyder, S.A. Sabbagh, H.W. Kuget, E.A. Unterberg, the NSTX Research Team: Elm triggering with 3d magnetic fields in nstx. Phys. Rev. Lett. **104**, 045001 (2009)

M.J. Choi, J.-M. Kwon, J. Kim, T. Rhee, J.-G. Bak, G. Shin, H.-S. Kim, H. Jhang, G.S.Y. K. Kim, M.W. Kim, S.K. Kim, H.H. Kaang, J.-K. Park, H.H. Lee, Y. In, J. Lee, M. Kim, B.-H. Park, H. Park, Stochastic fluctuation and transport of tokamak edge plasmas with the resonant magnetic perturbation field. Physics of Plasmas **29**(12), (2022)

M.J. Choi, J. Kim, J.-M. Kwon, H.K. Park, Y. In, W. Lee, K.D. Lee, G.S. Yun, J. Lee, M. Kim, W.-H. Ko, J.H. Lee, Y.S. Park, Y.-S. Na, N.C. Luhmann, B.H. Park, Multiscale interaction between a large scale magnetic island and small scale turbulence. Nucl. Fusion **57**(12), 126058 (2017)

A.J. Cole, R. Fitzpatrick, Drift-magnetohydrodynamical model of error-field penetration in tokamak plasmas. Phys. Plasmas **13**, 032503 (2006)

A.J. Cole, C.C. Hegna, J.D. Callen, Neoclassical toroidal viscosity and error-field penetration in tokamaks. Phys. Plasmas **15**, 056102 (2008)

J.W. Connor, A review of models for elms. Plasma Phys. Control. Fusion **40**, 191–213 (1998)

J.W. Connor, R.J. Hastie, Scaling laws for plasma confinement. Nucl. Fusion **13**, 221 (1973)

T.E. Evans, Resonant magnetic perturbations of edge-plasmas in toroidal confinement devices. Plasma Phys. Control. Fusion **57**, 123001 (2015)

T.E. Evans, R.A. Moyer, P.R. Thomas, J.G. Watkins, T.H. Osborne, J.A. Boedo, E.J. Doyle, M.E. Fenstermacher, K.H. Finken, R.J. Groebner, M. Groth, J.H. Harris, R.J. La Haye, C.J. Lasnier, S. Masuzaki, N. Ohyabu, D.G. Pretty, T.L. Rhodes, H. Reimerdes, D.L. Rudakov, M.J. Schaffer, G. Wang, L. Zeng, Suppression of large edge-localized modes in high-confinement diii-d plasmas with a stochastic magnetic boundary. Phys. Rev. Lett. **92**, 235003 (2004)

T.E. Evans, R.A. Moyer, J.G. Watkins, T.H. Osborne, P.R. Thomas, M. Becoulet, J.A. Boedo, E.J. Doyle, M.E. Fenstermacher, K.H. Finken, R.J. Groebner, M. Groth, J.H. Harris, G.L. Jackson, R.J. LaHaye, C.J. Lasnier, S. Masuzaki, N. Ohyabu, D.G. Pretty, H. Reimerdes, T.L. Rhodes, D.L. Rudakov, M.J. Schaffer, M.R. Wade, G. Wang, W.P. West, L. Zeng, Suppression of large edge-localized modes with edge resonant magnetic fields in high confinement diii-d plasmas. Nucl. Fusion **45**, 595 (2005)

T.E. Evans, R.A. Moyer, K.H. Burrell, M. Fenstermacher, I. Joseph, A.W. Leonard, T.H. Osborne, G.D. Porter, M.J. Schaffer, P.B. Snyder, P.R. Thomas, J.G. Watkins, W.P. West, Edge stability and transport control with resonant magnetic perturbations in collisionless tokamak plasmas. Nat. Phys. **2**, 419–423 (2006)

T.E. Evans, M.E. Fenstermacher, A. Moyer, T.H. Osborne, J.G. Watkins, P. Gohil, I. Joseph, M.J. Schaffer, L.R. Baylor, M. Bécoulet, J.A. Boedo, K.H. Burrell, J.S. deGrassie, K.H. Finken, T.

Jernigan, M.W. Jakubowski, C.J. Lasnier, M. Lehnen, A.W. Leonard, J. Lonnroth, E. Nardon, V. Parail, O. Schmitz, B. Unterberg, W.P. West, Rmp elm suppression in diii-d plasmas with iter similar shapes and collisionalities. Nucl. Fusion **48**, 024002 (2008)

Y. Feng, F. Sardei, J. Kisslinger, P. Grigull, A 3d monte carlo code for plasma transport in island divertors. J. Nucl. Mater. **241–243**, 930 (1997)

M.E. Fenstermacher, T.E. Evans, T.H. Osborne, M.J. Schaffer, M.P. Aldan, J.S. deGrassie, P. Gohil, I. Joseph, R.A. Moyer, P.B. Snyder, R.J. Groebner, M. Jakubowski, A.W. Leonard, O. Schmitz, the DIII-D Team: Effect of island overlap on edge localized mode suppression by resonant magnetic perturbations in diii-d. Phys. Plasmas **15**, 056122 (2008)

G.M. Fishpool, P.S. Haynes, Field error instabilities in jet. Nucl. Fusion **34**, 109 (1994)

R. Fitzpatrick, Interaction of tearing modes with external structures in cylindrical geometry. Nucl. Fusion **33**, 1049 (1993)

R. Fitzpatrick, Nonlinear error-field penetration in low density ohmically heated tokamak plasmas. Plasma Phys. Control. Fusion **54**, 094002 (2012)

R. Fitzpatrick, A neoclassical drift-magnetohydrodynamical fluid model of the interaction of a magnetic island chain with a resonant error-field in a high temperature tokamak plasma. Phys. Plasmas **25**, 042503 (2018)

R. Fitzpatrick, Nonlinear neoclassical two-fluid theory of response of tokamak plasma to resonant error-field. Phys. Plasmas **25**, 082513 (2018)

R. Fitzpatrick, T.C. Hender, The interaction of resonant magnetic perturbations with rotating plasmas. Phys. Fluids B **3**, 644–673 (1991)

R. Fitzpatrick, F.L. Waelbroeck, Two-fluid magnetic island dynamics in slab geometry. Phys. Plasmas **12**, 022307 (2005)

R. Fitzpatrick, F.L. Waelbroeck, Drift-tearing magnetic islands in tokamak plasmas. Phys. Plasmas **15**, 012502 (2008)

R. Fitzpatrick, F.L. Waelbroeck, Effect of flow damping on drift-tearing magnetic islands in tokamak plasmas. Phys. Plasmas **16**, 072507 (2009)

R. Fitzpatrick, Scaling of forced magnetic reconnection in the hall-magnetohydrodynamic taylor problem. Phys. Plasmas **11**, 937 (2004)

R. Fitzpatrick, An improved neoclassical drift-magnetohydrodynamical fluid model of helical magnetic island equilibria in tokamak plasmas. Phys. Plasmas **23**, 052506 (2016)

H. Frerichs, D. Reiter, O. Schmitz, T.E. Evans, Y. Feng, Three-dimensional edge transport simulations for diii-d plasmas with resonant magnetic perturbations. Nucl. Fusion **50**, 034004 (2010)

S. Gu, C. Paz-Soldan, Y.Q. Liu, Y. Sun, B.C. Lyons, D.A. Ryan, D. Weisberg, N. Leuthold, M. Willensdorfer, W. Suttrop, J.-K. Park, N.C. Logan, M.W. Shafer, H.H. Wang, Q. Ma, A. Kirk, B. Tal, M. Griener, the ASDEX Upgrade, the EUROfusion MST1 Teams: Influence of triangularity on the plasma response to resonant magnetic perturbations. Nucl. Fusion **62**, 076031 (2022)

R. Hager, C.S. Chang, N.M. Ferraro, R. Nazikian, Gyrokinetic understanding of the edge pedestal transport driven by resonant magnetic perturbations in a realistic divertor geometry. Phys. Plasmas **27**, 062301 (2020)

T.S. Hahm, Y.J. Kim, P.H. Diamond, G.J. Choi, Anisotropic exb shearing rate in a magnetic island. Phys. Plasmas **28**(2), 022302 (2021)

D.M. Harting, Y. Liang, S. Jachmich, R. Koslowski, G. Arnoux, S. Devaux, T. Eich, E. Nardon, D. Reiter, H. Thomsen, Strike point splitting in the heat and particle flux profiles compared with the edge magnetic topology in a n=2 resonant magnetic perturbation field at jet. Nuc. Fusion **52**(5), 054009 (2012)

R.J. Hawryluk, D.J. Campbell, G. Janeschitz, P.R. Thomas, R. Albanese, R. Ambrosino, C. Bachmann, L. Baylor, M. Becoulet, I. Benfatto, J. Bialek, A. Boozer, A. Brooks, R. Budny, T. Casper, M. Cavinato, J.-J. Cordier, V. Chuyanov, E. Doyle, T. Evans, G. Federici, M. Fenstermacher, H. Fujieda, K. Gal, A. Garofalo, L. Garzotti, D. Gates, Y. Gribov, P. Heitzenroeder, T.C. Hender, N. Holtkamp, D. Humphreys, I. Hutchinson, K. Ioki, J. Johner, G. Johnson, Y. Kamada, A. Kavin, C. Kessel, R. Khayrutdinov, G. Kramer, A. Kukushkin, K. Lackner, I. Landman, P. Lang, Y. Liang, J. Linke, B. Lipschultz, A. Loarte, G.D. Loesser, C. Lowry, T. Luce, V. Lukash, S. Maruyama, M. Mattei, J. Menard, M. Merola, A. Mineev, N. Mitchell, E. Nardon, R. Nazikian, B. Nelson, C. Neumeyer, J.-K. Park, R. Pearce, R.A. Pitts, A. Polevoi, A. Portone, M. Okabayashi, P.H. Rebut, V. Riccardo, J. Roth, S. Sabbagh, G. Saibene, G. Sannazzaro, M. Schaffer, M. Shimada, A. Sen, A. Sips, C.H. Skinner, P. Snyder, R. Stambaugh, E. Strait, M. Sugihara, E. Tsitrone, J. Urano, M.

Valovic, M. Wade, J. Wesley, R. White, D.G. Whyte, S. Wu, M. Wykes, L. Zakharov, Principal physics developments evaluated in the iter design review. Nucl. Fusion **49**, 065012 (2009)

R.D. Hazeltine, M. Kotschenreuther, P.J. Morrison, A four-field model for tokamak plasma dynamics. Phys. Fluids **28**, 2466 (1985)

P. Helander, C.D. Beidler, T.M. Bird, M. Drevlak, Y. Feng, R. Hatzky, F. Jenko, R. Kleiber, J.H.E. Proll, Y. Turkin, P. Xanthopoulos, Plasma Phys. Control. Fusion **54**, 124009 (2012)

T.C. Hender, R. Fitzpatrick, A.W. Morris, P.G. Carolan, R.D. Durst, T. Eddlington, J. Ferreira, S.J. Fielding, P.S. Haynes, J. Hugill, I.J. Jenkins, R.J. La Haye, B.J. Parham, D.C. Robinson, T.N. Todd, M. Valovic, G. Vayakis, Effect of resonant magnetic perturbations on compass-c tokamak discharges. Nucl. Fusion **32**, 2091 (1992)

W.A. Hornsby, P. Migliano, R. Buchholz, S. Grosshauser, A. Weikl, D. Zarzoso, F.J. Casson, E. Poli, A.G. Peeters, The non-linear evolution of the tearing mode in electromagnetic turbulence using gyrokinetic simulations. Plasma Phys. Control. Fusion **58**(1), 014028 (2015)

Q. Hu, R. Nazikian, B.A. Grierson, N.C. Logan, J.-K. Park, C. Paz-Soldan, Q. Yu, Phys. Plasmas **26**, 120702 (2019)

Q. Hu, N.C. Logan, J.-K. Park, C. Paz-Soldan, R. Nazikian, Q. Yu, Nonlinear modeling of the scaling law for the m/n = 3/2 error field penetration threshold. Nucl. Fusion **60**, 076006 (2020)

Q. Hu, R. Nazikian, B.A. Grierson, N.C. Logan, D.M. Orlov, C. Paz-Soldan, Q. Yu, Wide operational windows of edge-localized mode suppression by resonant magnetic perturbations in the diii-d tokamak. Phys. Rev. Lett. **125**, 045001 (2020)

Q. Hu, R. Nazikian, B.A. Grierson, N.C. Logan, C. Paz-Soldan, Q. Yu, The role of edge resonant magnetic perturbations in edge-localized-mode suppression and density pump-out in low-collisionality diii-d plasmas. Nucl. Fusion **60**, 076001 (2020)

Q.M. Hu, J.-K. Park, N.C. Logan, S.M. Yang, B.A. Grierson, R. Nazikian, Q. Yu, Nonlinear two-fluid modeling of plasma response to rmps for the elm control in the iter baseline. Nucl. Fusion **61**, 106006 (2021)

Q.M. Hu, R. Nazikian, N.C. Logan, J.-K. Park, C. Paz-Soldan, S.M. Yang, B.A. Grierson, Y. In, Y.M. Jeon, M. Kim, S.K. Kim, D.M. Orlov, G.Y. Park, Q. Yu, Predicting operational windows of elms suppression by resonant magnetic perturbations in the diii-d and kstar tokamaks. Phys. Plasmas **28**, 052505 (2021)

B. Hudson, T. Evans, C. Petty, P. Synder, Dependence of resonant magnetic perturbation experiments on the diii-d plasma shape. Nucl. Fusion **50**, 064005 (2010)

G.T.A. Huijsmans, A. Loarte, Non-linear mhd simulation of elm energy deposition. Nucl. Fusion **53**, 123023 (2013)

K. Ida, T. Kobayashi, M. Ono, T.E. Evans, G.R. McKee, M.E. Austin, Hysteresis relation between turbulence and temperature modulation during the heat pulse propagation into a magnetic island in diii-d. Phys. Rev. Lett. **120**, 245001 (2018)

Y. In, J.-K. Park, Y.M. Jeon, J. Kim, G.Y. Park, J.-W. Ahn, A. Loarte, W.H. Ko, H.H. Lee, J.W. Yoo, J.W. Juhn, S.W. Yoon, H. Park, Enhanced understanding of non-axisymmetric intrinsic and controlled field impacts in tokamaks. Nucl. Fusion **57**, 116054 (2017)

Y. In, Y.M. Jeon, J.-K. Park, A. Loarte, J.-W. Ahn, J.H. Lee, H.H. Lee, G.Y. Park, K. Kim, W.H. Ko, T. Rhee, J. Kim, S.W. Yoon, H. Park, 3D Physics Task Force in KSTAR: Tamed stability and transport using controlled non-axisymmetric fields in kstar. Nucl. Fusion **59**, 056009 (2019)

A. Ishizawa, Y. Kishimoto, Y. Nakamura, Multi-scale interactions between turbulence and magnetic islands and parity mixture - a review. Plasma Phys. Control. Fusion **61**, 056006 (2019)

M.W. Jakubowski, T.E. Evans, M.E. Fenstermacher, M. Groth, C.J. Lasnier, A.W. Leonard, O. Schmitz, J.G. Watkins, T. Eich, W. Fundamenski, R.A. Moyer, R.C. Wolf, L.B. Baylor, J.A. Boedo, K.H. Burrell, H. Frerichs, J.S. de Grassie, P. Gohil, I. Joseph, S. Mordijck, M. Lehnen, C.C. Petty, R.I. Pinsker, D. Reiter, T.L. Rhodes, U. Samm, M.J. Schaffer, P.B. Snyder, H. Stoschus, T. Osborne, B. Unterberg, E. Unterberg, W.P. West, Overview of the results on divertor heat loads in RMP controlled h-mode plasmas on DIII-d. Nucl. Fusion **49**(9), 095013, (2009)

Y.M. Jeon et al., Suppression of edge localized modes in high-confinement kstar plasmas by non-axisymmetric magnetic perturbations. Phys. Rev. Lett. **109**, 035004 (2012)

S.K. Kim, S. Pamela, O. Kwon, M. Becoulet, G.T.A. Huijsmans, Y. In, M. Hoelzl, J.H. Lee, M. Kim, G.Y. Park, H.S. Kim, Y.H. Lee, G.J. Choi, C.Y. Lee, A. Kirk, A. Thornton, JOREK team, Y.-S. Na, Nonlinear modeling of the effect of n=2 resonant magnetic field perturbation on peeling-ballooning modes in kstar. Nucl. Fusion **60**, 026009 (2020)

S.K. Kim, S. Pamela, O. Kwon, G. Huijsmans, Y. In, J. Lee, M.W. Kim, Y.-S. Na, On effect of n=2 rmp to edge pedestal in kstar with nonlinear mhd simulation. In: Proceedings of the 28th IAEA Fusion Energy Conference, p. 2. IAEA (2021)

K. Kim, J.-K. Park, A.H. Boozer, Numerical verification of bounce-harmonic resonances in neoclassical toroidal viscosity for tokamaks. Phys. Rev. Lett. **110**, 185004 (2013)

S.K. Kim, R. Shousha, S.H. Hahn, A.O. Nelson, J. Wai, S.M. Yang, J.-K. Park, R. Nazikian, N.C. Logan, Y.M. Jeon, Y. In, J.H. Lee, J. Kim, C.Y. Lee, Y.-S. Na, E. Kolemen, Optimization of 3d controlled elm-free state with recovered global confinement for kstar with n = 1 resonant magnetic field perturbation. Nucl. Fusion **62**, 026043 (2022)

A. Kirk, E. Nardon, R. Akers, M. Becoulet, G.D. Temmerman, B. Dudson, B. Hnat, Y.Q. Liu, R. Martin, P. Tamain, D. Taylor, the MAST team: resonant magnetic perturbation experiments on mast using external and internal coils for elm control. Nucl. Fusion **50**, 034008 (2010)

A. Kirk, J. Harrison, Y. Liu, E. Nardon, I.T. Chapman, P. Denner, the MAST Team: observation of lobes near the x point in resonant magnetic perturbation experiments in mast. Phys. Rev. Lett. **108**, 255003 (2012)

A. Kirk, I.T. Chapman, Y. Liu, P. Cahyna, P. Denner, G. Fishpool, C.J. Ham, J.R. Harrison, Y. Liang, E. Nardon, S. Saarelma, R. Scannell, A.J. Thornton, the MAST team: Understanding edge-localized mode mitigation by resonant magnetic perturbations on mast. Nucl. Fusion **53**, 043007 (2013)

A. Kirk, W. Suttrop, I.T. Chapman, Y. Liu, A.J.T. Rscannell, L. BarreraOrte, P. Cahyna, T. Eich, R. Fischer, C. Fuchs, C. Ham, J.R. Harrison, M.W. Jakubowski, B. Kurzan, S. Pamela, M. Peterka, D. Ryan, S. Saarelma, B. Sieglin, M. Valovic, M. Willensdorfer, MAST and ASDEX Upgrade Teams: Effect of resonant magnetic perturbations on low collisionality discharges in mast and a comparison with asdex upgrade. Nucl. Fusion **55**, 043011 (2015)

J.-M. Kwon, S. Ku, M.-J. Choi, C.S. Chang, R. Hager, E.S. Yoon, H.H. Lee, H.S. Kim, Gyrokinetic simulation study of magnetic island effects on neoclassical physics and micro-instabilities in a realistic kstar plasma. Phys. Plasmas **25**(5), 052506 (2018)

R.J. La Haye, R. Fitzpatrick, T.C. Hender, A.W. Morris, J.T. Scoville, T.N. Todd, Non-linear instability to low m, n=1 error fields in diii-d as a function of plasma fluid rotation and beta. Phys. Fluids B **4**, 2098 (1992)

M.J. Lanctot, H. Reimerdes, A.M. Garofalo, M.S. Chu, Y.Q. Liu, E.J. Strait, G.L. Jackson, R.J. La Haye, M. Okabayashi, T.H. Osborne, M.J. Schaffer, Validation of the linear ideal magnetohydrodynamic model of three-dimensional tokamak equilibria. Phys. Plasmas **17**, 030701 (2010)

M.J. Lanctot, H. Reimerdes, A.M. Garofalo, M.S. Chu, J.M. Hanson, Y.Q. Liu, G.A. Navratil, I.N. Bogatu, Y. In, G.L. Jackson, R.J.L. Haye, M. Okayabashi, J.-K. Park, M.J. Schaffer, O. Schmitz, E.J. Strait, A.D. Turnbull, Measurement and modeling of three-dimensional equilibria in diii-d. Phys. Plasmas **18**, 056121 (2011)

M.J. Lanctot, J.-K. Park, P. Piovesan, Y. Sun, R.J. Buttery, L. Frassubetti, B.A. Grierson, J.M. Hanson, S.R. Haskey, Y. In, Y.M. Jeon, R.J. La Haye, N.C. Logan, L. Marrelli, D.M. Orlov, C. Paz-Soldan, H.H. Wang, E.J. Strait, JET Contributors, Impact of toroidal and poloidal mode spectra on the control of non-axisymmetric fields in tokamaks. Phys. Plasmas **24**, 056117 (2017)

S.A. Lazerson, J.-K. Park, N.C. Logan, A.H. Boozer, Numerical optimization of three-dimensional coils for nstx-u. Plasma Phys. Control. Fusion **57**, 104001 (2015)

G.S. Lee et al., The kstar project: An advanced steady state superconducting tokamak experiment. Nucl. Fusion **40**, 575–582 (2000)

J. Lee, G.S. Yun, M.J. Choi, J.-M. Kwon, Y.M. Jeon, W. Lee, N.C. Luhmann Jr., H.K. Park, Nonlinear interaction of edge-localized modes and turbulent eddies in toroidal plasma under n = 1 magnetic perturbation. Phys. Rev. Lett. **117**, 075001 (2016)

Y. Liang, H.R. Koslowski, P.R. Thomas, E. Nardon, B. Alper, P. Andrew, Y. Andrew, G. Arnoux, Y. Baranov, M. Bécoulet, M. Beurskens, T. Biewer, M. Bigi, K. Crombe, E. De La Luna, P. de Vries, W. Fundamenski, S. Gerasimov, C. Giroud, M.P. Gryaznevich, N. Hawkes, S. Hotchin, D. Howell, S. Jachmich, V. Kiptily, L. Moreira, V. Parail, S.D. Pinches, E. Rachlew, O. Zimmermann, Active control of type-i edge-localized modes with n=2 perturbation fields in the jet tokamak. Phys. Rev. Lett. **98**, 265004 (2007)

Y. Liu, B.C. Lyons, S. Gu, A. Kirk, L. Li, C. Paz-Soldan, Shafer, M.W., Turnbull, A.D.: Influence of up-down asymmetry in plasma shape on rmp response. Plasma Phys. Control. Fusion 63, 065003 (2021)

Y. Liu, A. Kirk, L. Li, Y. In, R. Nazikian, Y. Sun, W. Suttrop, B. Lyons, D. Ryan, S. Wang, X. Yang, L. Zhou, EUROfusionMST1 team: Comparative investigation of elm control based on toroidal modelling of plasma response to rmp fields. Phys. Plasmas **24**, 056111 (2017)

Y. Liu, C. Paz-Soldan, L. Li, Y. Sun, Role of 3d neoclassical particle flux in density pump-out during elm control by rmp in diii-d. Nucl. Fusion **60**, 036018 (2020)

A. Loarte, G. Huijsmans, S. Futatani, L.R. Baylor, T.E. Evans, D.M. Orlov, O. Schmitz, M. Becoulet, P. Cahyna, Y. Gribov, A. Kavin, A. Sashala Naik, D.J. Campbell, T. Casper, E. Daly, H. Frerichs, A. Kischner, R. Laengner, S. Lisgo, R.A. Pitts, G. Saibene, A. Wingen, Progress on the application of elm control schemes to iter scenarios from the non-active phase to dt operation. Nucl. Fusion **54**, 033007 (2014)

N.C. Logan, J.-K. Park, K. Kim, Z.R. Wang, J.W. Berkery, Neoclassical toroidal viscosity in perturbed equilibria with general tokamak geometry. Plasma Phys. **20**, 122507 (2013)

N.C. Logan, J.-K. Park, Q. Hu, C. Paz-Soldan, T. Markovic, H.H. Wang, Y. In, L. Piron, P. Piovesan, C.E. Myers, M. Maraschek, S.M. Wolfe, E.J. Strait, S. Munaretto, Empirical scaling of the n=2 error field penetration threshold in tokamaks. Nucl. Fusion **60**, 086010 (2020)

N.C. Logan, C. Zhu, J.-K. Park, S.M. Yang, Q. Hu, Physics basis for design of 3d coils in tokamaks. Nucl. Fusion **61**, 076010 (2021)

J.D. Lore, A.R. Briesemeister, N.M. Ferraro, H. Frerichs, B. Lyons, A. McLean, J.-K. Park, M.W. Shafer, Pedestal-to-wall 3d fluid transport simulations on DIII-d. Nucl. Fusion **57**(5), 056025 (2017)

J.L. Luxon, M.J. Schaffer, G.L. Jackson, J.A. Leuer, A. Nagy, J.T. Scoville, E.J. Strait, Tbr. Nucl. Fusion **43**, 1813 (2003)

T. Markovic, M. Peterka, A. Loarte, J.-K. Park, Y. Gribov, J. Havlicek, R. Panek, P. Hacek, M. Hron, M. Imrisek, K. Kovarik, L. Kripner, K. Mitosinkova, M. Sos, M. Tomes, J. Varju, P. Vondracek, V. Weinzettl, the COMPASS team http://ohttp://ocs.ciemat.es/EPS2018ABS/pdf/O3.108.pdf. in Proceedings of the 45th EPS Conference (2018)

G.R. McKee, Z. Yan, C. Holland, R.J. Buttery, T.E. Evans, R.A. Moyer, S. Mordijck, R. Nazikian, T.L. Rhodes, O. Schmitz, M.R. Wade, Increase of turbulence and transport with resonant magnetic perturbations in ELM-suppressed plasmas on DIII-d. Nucl. Fusion **53**(11), 113011 (2013)

J.E. Menard, R.E. Bell, D.A. Gates, S.P. Gerhardt, J.-K. Park, S.A. Sabbagh, J.W. Berkery, A. Egan, J. Kallman, S.M. Kaye, B. LeBlanc, Y.Q. Liu, A. Sontag, D. Swanson, H. Yuh, W. Zhu, the NSTX research team: progress in understanding error-field physics in nstx spherical torus plasmas. Nucl. Fusion **50**, 045008 (2010)

R.A. Moyer, T.E. Evans, T.H. Osborne, P.R. Thomas, M. Becoulet, J.H. Harris, K.-H. Finken, J.A. Boedo, E.J. Doyle, M.E. Fenstermacher, P. Gohil, R.J. Groebner, M. Groth, G.L. Jackson, R.J. LaHaye, C.J. Lasnier, A.W. Leonard, G.R. McKee, H. Reimerdes, T.L. Rhodes, D.L. Rudakov, M.J. Schaffer, P.B. Snyder, M.R. Wade, G. Wang, J.G. Watkins, W.P. West, L. Zeng, Edge localized mode control with an edge resonant magnetic perturbation. Phys. Plasmas **12**, 056119 (2005)

R.A. Moyer, C. Paz-Soldan, R. Nazikian, D.M. Orlov, N.M. Ferraro, B.A. Grierson, M. Knölker, B.C. Lyons, G.R. McKee, T.H. Osborne, T.L. Rhodes, O. Meneghini, S. Smith, T.E. Evans, M.E. Fenstermacher, R.J. Groebner, J.M. Hanson, R.J.L. Haye, T.C. Luce, S. Mordijck, W.M. Solomon, F. Turco, Z. Yan, L. Zeng, DIII-D Team: Validation of the model for elm suppression with 3d magnetic fields using low torque iter baseline scenario discharges in diii-d. Phys. Plasmas **24**, 102501 (2017)

R. Nazikian, W. Suttrop, A. Kirk, T. Evans, B.A. Grierson, R. McDermott, C. Paz-Soldan, D. Orlov, M. Willensdorfer. First observation of elm suppression in asdex-upgrade in a similarity experiment with diii-d. In: Proceedings of the 26th IAEA Fusion Energy Conference, pp. 1. IAEA (2016)

R. Nazikian, C. Paz-Soldan, J.D. Callen, J.S. deGrassie, D. Eldon, T.E. Evans, N.M. Ferraro, B.A. Grierson, R.J. Groebner, S.R. Haskey, C.C. Hegna, J.D. King, N.C. Logan, G.R. McKee, R.A. Moyer, M. Okabayashi, D.M. Orlov, T.H. Osborne, J.-K. Park, T.L. Rhodes, M.W. Shafer, P.B. Snyder, W.M. Solomon, E.J. Strait, M.R. Wade, Pedestal bifurcation and resonant field penetration at the threshold of edge-localized mode suppression in the diii-d tokamak. Phys. Rev. Lett. **114**, 105002 (2015)

C. Nürenberg, R. Zille, Quasihelically symmetric toroidal stellarators. Phys. Lett. A **129**, 113 (1988)

R. Orain, M. Hölzl, E. Viezzer, M. Dunne, M. Bécoulet, P. Cahyna, G.T.A. Huijsmans, J. Morales, M. Willensdorfer, W. Suttrop, A. Kirk, S. Pamela, S. Günter, K. Lackner, E. Strumberger, A. Lessig, the ASDEX Upgrade team, the EUROfusion MST1 Team: Non-linear modeling of the plasma response to rmps in asdex upgrade. Nucl. Fusion **57**, 022013 (2017)

G. Park, Y. In, J.-K. Park, W.H. Ko, J. Lee, M. W. G.W.S. Kim, S.-H. Hahn, S.K. Kim, S.M. Yang, Q. Hu, T. Rhee, M.J. Choi, K. Kim, H.H. Lee, Y.M. Jeon, W.-C. Kim, S.W. Yoon, Overview of recent progress in 3d field physics in kstar. J. Korean Phys. Soc. **80**, 759 (2022)

J.-K. Park, N.C. Logan, Self-consistent perturbed equilibrium with neoclassical toroidal torque in tokamaks. Phys. Plasmas **24**, 032505 (2017)

J.-K. Park, M.J. Schaffer, J.E. Menard, A.H. Boozer, Control of asymmetric magnetic perturbations in tokamaks. Phys. Rev. Lett. **99**, 195003 (2007)

J.-K. Park, A.H. Boozer, J.E. Menard, Spectral asymmetry due to magnetic coordinates. Phys. Plasmas **15**, 064501 (2008)

J.-K. Park, A.H. Boozer, J.E. Menard, Non-ambipolar transport by trapped particles in tokamaks. Phys. Rev. Lett. **102**, 065002 (2009)

G. Park, C.S. Chang, I. Joseph, R.A. Moyer, Plasma transport in stochastic magnetic field caused by vacuum resonant magnetic perturbations at diverted tokamak edge. Phys. Plasmas **17**, 102503 (2010)

J.-K. Park, Y.M. Jeon, J.E. Menard, W.H. Ko, S.G. Lee, Y.S. Bae, M. Joung, K.-I. You, K.-D. Lee, N.C. Logan, K. Kim, J.S. Ko, S.W. Yoon, S.H. Hahn, J.H. Kim, W.C. Kim, Y.-K. Oh, J.-G. Kwak, Rotational resonance of nonaxisymmetric magnetic braking in the kstar tokamak. Phys. Rev. Lett. **111**, 095002 (2013)

J.-K. Park, Y.M. Jeon, Y. In, J.-W. Ahn, R. Nazikian, G. Park, J. Kim, H.H. Lee, W.H. Ko, N.C. Logan, Z. Wang, E.A. Feibush, J.E. Menard, M.C. Zarnstorff, 3d field phase-space control in tokamak plasmas. Nat. Phys. **14**, 1223–1228 (2018)

J.-K. Park, S.M. Yang, N.C. Logan, Q. Hu, C. Zhu, M.C. Zarnstorff, R. Nazikian, C. Paz-Soldan, Y.M. Jeon, W.H. Ko, Quasisymmetric optimization of nonaxisymmetry in tokamaks. Phys. Rev. Lett. **126**, 125001 (2021)

C. Paz-Soldan, M.J. Lanctot, N.C. Logan, D. Shiraki, R.J. Buttery, J.M. Hanson, R.J. La Haye, J.-K. Park, W.M. Solomon, E.J. Strait, The importance of matched poloidal spectra to error field correction in diii-d. Phys. Plasmas **21**, 072503 (2014)

C. Paz-Soldan, R. Nazikian, S.R. Haskey, N.C. Logan, E.J. Strait, N.M. Ferraro, J.M. Hanson, J.D. King, M.J. Lanctot, R.A. Moyer, M. Okabayashi, J.-K. Park, M.W. Shafer, B.J. Tobias, Observation of a multimode plasma response and its relationship to density pumpout and edge-localized mode suppression. Phys. Rev. Lett. **114**, 105001 (2015)

C. Paz-Soldan, R. Nazikian, L. Cui, B.C. Lyons, D.M. Orlov, A. Kirk, N.C. Logan, T.H. Osborne, W. Suttrop, D.B. Weisberg, The effect of plasma shape and neutral beam mix on the rotation threshold for rmp-elm suppression. Nucl. Fusion **59**, 056012 (2019)

E. Poli, A. Bottino, A.G. Peeters, Behaviour of turbulent transport in the vicinity of a magnetic island. Nucl. Fusion **49**, 075010 (2009)

T. Rhee, J. Kim, K. Kim, J. Kang, M. Podesta, Y.-S. Park, B.-H. Park, Simulation study of fast ion losses associated with the rotating n = 1 resonant magnetic perturbations in kstar. Nucl. Fusion **62**, 066028 (2022)

P.H. Rutherford, Nonlinear growth of the tearing mode. Phys. Fluid **16**, 1903 (1973)

M.J. Schaffer, J.E. Menard, M.P. Aldan, J.M. Bialek, T.E. Evans, R.A. Moyer, Study of in-vessel nonaxisymmetric elm suppression coil concepts for iter. Nucl. Fusion **48**, 024004 (2008)

O. Schmitz, T.E. Evans, M.E. Fenstermacher, A. McLean, J. Boedo, N.H. Brooks, H. Frerichs, M. Jakubowski, R. Laengner, C.L. Lasnier, A. Loarte, R.A. Moyer, D. Orlov, H. Reimerdes, D. Reiter, U. Samm, H. Stoschus, E.A. Unterberg, J.G. Watkins, The influence of three-dimensional stochastic magnetic boundaries on plasma edge transport and the resulting plasma wall interaction. J. Nucl. Mater. **415**(1, Supplement), 886–893 (2011)

J.T. Scoville, R.J. LaHaye, Multi-mode error field correction on the diii-d tokamak. Nucl. Fusion **43**, 250 (2003)

M.W. Shafer, C. Paz-Soldan, T.E. Evans, N. Ferraro, B. Lyons, T. Osborne, A. Turnbull. Limits of rmp elm suppression in double null plasmas. In: Proceedings of the 28th IAEA Fusion Energy Conference, pp. 1–930. IAEA (2021)

K.C. Shaing, Neoclassical flows and transport in non-axisymmetric toroidal plasmas. Phys. Fluids **26**, 3315–3326 (1983)

K.C. Shaing, Symmetry-breaking induced transport in the vicinity of a magnetic island. Phys. Rev. Lett. **87**, 245003 (2001)

K.C. Shaing, Magnetohydrodynamic-activity-induced toroidal momentum dissipation in collisionless regimes in tokamaks. Phys. Plasmas **10**, 1443 (2003)

K.C. Shaing, P. Cahyna, M. Becoulet, J.-K. Park, S.A. Sabbagh, M.S. Chu, Collisional boundary layer analysis for neoclassical toroidal plasma viscosity in tokamaks. Phys. Plasmas **15**, 082506 (2008)

K.C. Shaing, K. Ida, S.A. Sabbagh, Neoclassical plasma viscosity and transport processes in non-axisymmetric neoclassical plasma viscosity and transport processes in non-axisymmetric tori. Nucl. Fusion **55**, 125001 (2015)

T. Shoji, H. Tamai, Y. Miura, M. Mori, H. Ogawa, A.W. Leonard, T. Jensen, A.W. Hyatt, A.M. Howald, G. Fuchs, N. Ohyabu, N. Asakura, T. Fujita, M. Shimada, S. Tsuji, H. Maeda, H. Aikawa, K. Hoshino, S. Kasai, T. Kawakami, H. Kawashima, M. Maeno, T. Matsuda, T. Ogawa, T. Seike, N. Suzuki, K. Uehara, T. Yamamoto, T. Yamauchi, T. Hamano, K. Hasegawa, A. Honda, M. Kazawa, Y. Kashiwa, K. Kikuchi, H. Okano, E. Sato, N. Seki, T. Shibata, T. Shiina, S. Suzuki, T. Tani, T. Tokutake, Y. Tomiyama, T. Yamasato, Effects of ergodization on plasma confinement in jft-2m. Journal of Nucl. Materials **196–198**, 296–300 (1992)

R. Shousha, S.K. Kim, K.G. Erickson, S.H. Hahn, A.O. Nelson, S.M. Yang, J.-K. Park, J. Wai, Y.M. Jeon, J.H. Lee, J. Jang, D. Seo, E. Kolemen, Design and experimental demonstration of feedback adaptive rmp elm controller toward complete long pulse elm suppression on kstar. Phys. Plasmas **29**, 032514 (2022)

P.B. Snyder, K.H. Burrell, H.R. Wilson, M.S. Chu, M.E. Fenstermacher, A.W. Leonard, R.A. Moyer, T.H. Osborne, M. Umansky, W.P. West, X.Q. Xu, Stability and dynamics of the edge pedestal in the low collisionality regime: physics mechanisms for steady-state elm-free operation. Nucl. Fusion **47**, 961–968 (2007)

Y. Sun, Y. Liang, K.C. Shaing, H.R. Koslowski, C. Wiegmann, T. Zhang, Neoclassical toroidal plasma viscosity torque in collisionless regimes in tokamaks. Phys. Rev. Lett. **105**, 145002 (2010)

Y. Sun, Y. Liang, K.C. Shaing, Y.Q. Liu, H.R. Koslowski, S. Jachmich, B. Alper, A. Alfier, O. Asunta, P. Buratti, G. Corrigan, E. Delabie, C. Giroud, M.P. Gryaznevich, D. Harting, T. Hender, E. Nardon, V. Naulin, V. Parail, T. Tala, C. Wiegmann, S. Wiesen, T. Zhang, JET-EFDA contributors: Non-resonant magnetic braking on jet and textor. Nucl. Fusion **52**, 083007 (2012)

Y. Sun, Y. Liang, Y.Q. Liu, S. Gu, X. Yang, W. Guo, T. Shi, M. Jia, L. Wang, B. Lyu, C. Zhou, A. Liu, Q. Zang, H. Liu, N. Chu, H.H. Wang, T. Zhang, J. Qian, L. Xu, K. He, D. Chen, B. Shen, X. Gong, X. Ji, S. Wang, M. Qi, Y. Song, Q. Yuan, Z. Sheng, G. Gao, P. Fu, B. Wan, Nonlinear transition from mitigation and suppression of the edge localized mode with resonant magnetic perturbations in the east tokamak. Phys. Rev. Lett. **117**, 115001 (2016)

W. Suttrop, T. Eich, J.C. Fuchs, S. Gunter, A. Janzer, A. Herrmann, A. Kallenbach, P.T. Lang, T. Lunt, M. Maraschek, R.M. McDermott, A. Mlynek, T. Putterich, M. Rott, T. Vierle, E. Wolfrum, Q. Yu, I. Zammuto, H. Zohm, ASDEX Upgrade Team: First observation of edge localized modes mitigation with resonant and nonresonant magnetic perturbations in asdex upgrade. Phys. Rev. Lett. **106**, 225004 (2011)

W. Suttrop, A. Kirk, R. Nazikian, N. Leuthold, E. Strumberger, M. Willensdorfer, M. Cavedon, M. Dunne, R. Fischer, S. Fietz, J.C. Fuchs, Y.Q. Liu, R.M. McDermott, F. Orain, D.A. Ryan, E. Viezzer, The ASDEX Upgrade Team, The DIII-D Team, The Eurofusion MST1 Team: Experimental studies of high-confinement mode plasma response to non-axisymmetric magnetic perturbations in asdex upgrade. Plasma Phys. Control. Fusion **59**, 014049 (2017)

W. Suttrop, A. Kirk, V. Bobkov, M. Cavedon, M. Dunne, R.M. McDermott, H. Meyer, R. Nazikian, C. Paz-Soldan, D.A. Ryan, E. Viezzer, M. Willensdorfer, The ASDEX Upgrade, MST1 Teams: Experimental conditions to suppress edge localised modes by magnetic perturbations in the asdex upgrade tokamak. Nucl. Fusion **58**, 096031 (2018)

S. Taimourzadeh, L. Shi, Z. Lin, R. Nazikian, I. Holod, D. Spong, Effects of rmp-induced changes of radial electric fields on microturbulence in diii-d pedestal top. Nucl. Fusion **59**, 046005 (2019)

M.A. Van Zeeland, N.M. Ferraro, B.A. Grierson, W.W. Heidbrink, G.J. Kramer, C.J. Lasnier, D.C. Pace, S.L. Allen, X. Chen, T.E. Evans, M. García-Muñoz, J.M. Hanson, M.J. Lanctot, L.L. Lao, W.H. Meyer, R.A. Moyer, R. Nazikian, D.M. Orlov, C. Paz-Soldan, A. Wingen, Fast ion transport during applied 3d magnetic perturbations on diii-d. Nucl. Fusion **55**, 073028 (2015)

M.R. Wade, R. Nazikian, J.S. deGrassie, T.E. Evans, N.M. Ferraro, R.A. Moyer, D.M. Orlov, R.J. Buttery, M.E. Fenstermacher, A.M. Garofalo, M.A. Lanctot, G.R. McKee, T.H. Osborne, M.A. Shafer, W.M. Solomon, P.B. Snyder, W. Suttrop, A. Wingen, E.A. Unterberg, L. Zeng, Advances in the physics understanding of elm suppression using resonant magnetic perturbations in diii-d. Nucl. Fusion **55**, 023002 (2015)

F.L. Waelbroeck, Shielding of resonant magnetic perturbations in the long mean-free path regime. Phys. Plasmas **10**, 4040 (2003)

F.L. Waelbroeck, I. Joseph, E. Nardon, M. Bécoulet, R. Fitzpatrick, Role of singular layers in the plasma response to resonant magnetic perturbations. Nucl. Fusion **52**, 074004 (2012)

F. Wagner, G. Fussmann, T. Grave, M. Keilhacker, M. Kornherr, K. Lackner, K. McCormick, E.R. Muller, A. Stabler, G. Becker, K. Bernhardi, U. Ditte, A. Eberhagen, O. Gehre, J. Gernhardt, v. G. Gierke, E. Glock, O. Gruber, G. Haas, M. Hesse, G. Janeschitz, F. Karger, S. Kissel, O. Kluber, G. Lisitano, H.M. Mayer, D. Meisel, V. Mertens, H. Murrmann, W. Poschenrieder, H. Rapp, H. Rohr, F. Ryter, F. Schneider, G. Siller, P. Smeulders, F. Soldner, E. Speth, K.-H. Steuer, Z. Szymanski, O. Vollmer, Development of an edge transport barrier at the h-mode transition of asdex. Phys. Rev. Lett. **53**, 1453 (1984)

R.E. Waltz, N.M. Ferraro, Theory and simulation of quasilinear transport from external magnetic field perturbations in a diii-d plasma. Phys. Plasmas **22**, 042507 (2015)

M. Willensdorfer, V. Mitterauer, G. Suarez, W. Suttrop, M.R. Cianciosa, M. Dunne, R. Fischer, M. Hoelzl, T. Gleiter, D. Wendler. Internal Plasma Response Measurements at the pedestal top in ELM suppressed plasmas in ASDEX Upgrade. 2022 APS invited talk, GL02.00005

S.M. Wolfe, I.H. Hutchinson, R.S. Granetz, J. Rice, A. Hubbard, A. Lynn, P. Phillips, T.C. Hender, D.F. Howell, R.J. La Haye, J.T. Scoville, Nonaxisymmetric field effects on alcator c-mod. Phys. Plasmas **12**, 056110 (2005)

Y. Xu, L. Li, Y. Hu, Y. Liu, W. Guo, L. Ye, X. Xiao, Numerical simulations of nbi fast ion loss with rmps on the east tokamak. Nucl. Fusion **60**, 086013 (2020)

S.M. Yang, J.-K. Park, N.C. Logan, C. Zhu, Q. Hu, Y.M. Jeon, Y. In, W.H. Ko, S.K. Kim, Y.H. Lee, Y.S. Na, Localizing resonant magnetic perturbations for edge localized mode control in kstar. Nucl. Fusion **60**, 096023 (2020)

Q. Yu, S. Gunter, Y. Kikuchi, K.H. Finken, Numerical modelling of error field penetration. Nucl. Fusion **48**, 024007 (2008)

W. Zhu, S.A. Sabbagh, R.E. Bell, J.M. Bialek, B.P. LeBlanc, S.M. Kaye, F.M. Levinton, J.E. Menard, K.C. Shaing, A.C. Sontag, H. Yuh, Observation of plasma toroidal-momentum dissipation by neoclassical toroidal viscosity. Phys. Rev. Lett. **96**, 225002 (2006)

C. Zhu, S.R. Hudson, Y. Song, Y. Wan, New method to design stellarator coils without the winding surface. Nucl. Fusion **58**, 016008 (2018)

H. Zohm, Edge localized modes (elms). Plasma Phys. Control. Fusion **38**, 105–128 (1996)

Authors and Affiliations

Jong-Kyu Park[1,2]

✉ Jong-Kyu Park
  jpark@pppl.gov

1   Princeton Plasma Physics Laboratory, Princeton, NJ 08543, USA

2   Department of Nuclear Engineering, Seoul National University, Seoul 08826, South Korea